geosciences

MDPI

Article

Spatiotemporal Variability Analysis of Rainfall and Water Quality: Insights from Trend Analysis and Wavelet Coherence Approach

Syeda Zehan Farzana [1,2,*], Dev Raj Paudyal [1,*], Sreeni Chadalavada [2] and Md Jahangir Alam [2,3]

[1] School of Surveying and Built Environment, University of Southern Queensland (UniSQ), Toowoomba, QLD 4350, Australia
[2] School of Engineering, University of Southern Queensland (UniSQ), Springfield Lakes, QLD 4300, Australia; sreeni.chadalavada@unisq.edu.au (S.C.); mdjahangir.alam@unisq.edu.au (M.J.A.)
[3] Murray-Darling Basin Authority (MDBA), Canberra, ACT 2601, Australia
* Correspondence: zehan.farzana@unisq.edu.au (S.Z.F.); devraj.paudyal@unisq.edu.au (D.R.P.)

Abstract: An understanding of the trend and relationship between rainfall patterns and water quality dynamics can provide valuable guidelines for the effective management of water resources. The aim of this study was to reveal the synchronous trends in rainfall and water quality and to explore the potential connection between seasonal variation in rainfall volume and the water quality index. This study scrutinised the seasonal temporal trends of rainfall and water quality parameters of three water supply reservoirs in the Toowoomba region of Australia by applying the modified Mann–Kendall (MMK) test and innovative trend analysis (ITA) methods from data collected over 22 years (2002–2022). The models showed a significant increasing trend of rainfall in two rainfall stations during autumn season. The water quality parameters, such as PO_4^{3-}, exhibited a significant decreasing trend in all seasons in three reservoirs. On the other hand, the water quality index (WQI) showed a decreasing trend in the Cooby and Cressbrook reservoirs, excepting the Perseverance reservoir, which exhibited an increasing trend. In addition to the detection of trends, this study investigated the potential correlation between seasonal variation of rainfall volume and the water quality index using the wavelet transform coherence (WTC) method. The data of twelve rainfall stations were brought into this analysis. The WTC analysis displayed an apparent correlation between the water quality index and rainfall pattern for 70% of the rainfall stations across 8–16 periods. The highest coherency was noticed in 8–16 periods from 2002–2022, as observed at both the Cooby Creek rainfall station and in the WQI of the Cooby reservoir. This evaluation revealed the intertwined dynamics of rainfall patterns and water quality, providing a deeper understanding of their interdependence and implications, which might be useful for environmental and hydrological management practices.

Keywords: rainfall; water quality; modified Mann–Kendall test; innovative trend analysis; wavelet transform coherence

Citation: Farzana, S.Z.; Paudyal, D.R.; Chadalavada, S.; Alam, M.J. Spatiotemporal Variability Analysis of Rainfall and Water Quality: Insights from Trend Analysis and Wavelet Coherence Approach. *Geosciences* **2024**, *14*, 225. https://doi.org/10.3390/geosciences14080225

Academic Editor: Gang Huang

Received: 9 July 2024
Revised: 9 August 2024
Accepted: 17 August 2024
Published: 21 August 2024

1. Introduction

Rainfall plays a crucial role in hydrological processes, and its spatial and temporal distribution, along with evolving characteristics, can significantly affect agriculture, ecosystems, and the management of water resources [1]. The understanding of monthly, seasonal, and annual variability of rainfall and as well as the severity of extreme rainfall and how it affects agriculture, ecosystem and water resources is crucial to ensure proper water resource management practices [2]. Rainfall patterns have changed significantly over recent years due to climate change leading to frequent flooding and drought. These events, in turn, have disrupted the ecosystem of water bodies and impacted the water quality [3]. With growing awareness about the escalating impact of climate change, it is important to grasp the characteristics and variations of rainfall, as well as how these patterns shift across

various spatial and temporal scales. Previous studies [4,5] have reported that there is global as well as regional scale change in rainfall patterns caused by global climate change.

Inland waters, such as rivers, lakes, reservoirs, and streams, provide diverse ecosystem services, from food sources to transportation channels and recreational sites. The deterioration of water quality due to the impact of extreme rainfall and rapid socio-economic development poses a significant environmental concern for inland water bodies [6]. Increases in extreme hydrological events and circulating (air) temperature are the dominant factors affecting water quality. Prolonged and heavy precipitation after drought periods then causes runoff and erosion that together consequently increase the pollutant release into surface water bodies [7]. Efforts to explore the efficacy of previous initiatives and the primary factors influencing the quality of inland water must continue to be thoroughly examined across different temporal and spatial dimensions. Among various nutrients present in water bodies, Nitrogen (N) and phosphorus (P) are two crucial elements that may disrupt the balance of aquatic ecosystems, thereby influencing diverse services such as navigation, water sports, fisheries and, most importantly, drinking water supply [8].

Time series data analysis is crucial for understanding the dynamics of events, which can play a key role in strategic infrastructure planning and early warning systems [9]. Hydroclimatic time series can display trends, whether upward or downward, and can locate change points that may relate to climate change influences, like increasing greenhouse gas levels, and alterations in land use and management practices [10–12]. To consider adaptation and mitigation strategies to counteract the effects of climate change and making informed decisions, it is essential to gain better understanding of trends and variability of hydroclimatic variables [13]. Precipitation concentration index (PCI), seasonality index (SI) and coefficient variation (CV) were extensively applied to examine the variability of rainfall, temperature and streamflow and to analyse the spatial and temporal distribution [14–16].

Over the past few years, there has been a growing need to periodically measure various water quality variables to monitor the status of surface water [17]. The steady collection of water quality records can provide a reliable synopsis of water quality status, identifying existing or potential water quality issues, understanding their causes, and evaluating the effectiveness of any implemented measures [17,18]. To date, numerous studies [19,20] have been conducted to explore the influences impacting changes in water quality such as pollution from agriculture, sewage discharge, socio-economic advancements, water consumption, and forest and climate extremes. Among all other variables, climate extremes are expected to significantly influence future hydrological patterns, affecting various sectors that depend on surface water. Delpla et al. [21] showed that the amount of organic matter was likely to increase in streams that experienced an increased volume of rainfall and alterations in drought-rewetting cycles. Consequently, Ponting et al. [22] discovered that inorganic and organic matter were carried into rivers by flood water, whereas Ockenden et al. [23] showed a positive trend and correlation between annual rainfall and total phosphorus load. Moreover, Mortazavi-Naeini et al. [24] have demonstrated a positive relationship between extreme winter rainfall and suspended sediment concentration and an elevated level of phosphorus during the low flow period. Additionally, Watts and Anderson [25] observed that a reduction in summer flow is expected to decrease the dissolved oxygen level and conversely, high summer floods to enhance the concentration of nutrients and pollutants in the river system. Nevertheless, despite the above studies offering basic theoretical frameworks and empirical illustrations of the source of water quality change, there are still notable shortcomings. Because of inadequate data sources and diverse research objectives, the systematic formation of the correlation between water quality parameters and key driving factors has not yet been undertaken. This limitation hinders support for the prevention of water quality deterioration in areas facing significant water quality issues [26,27].

In recent decades, various methods have been developed and used for analysing trends in time series such as the Mann–Kendall (MK) test, seasonal Kendall methods, the modified Mann–Kendall (MMK) test, linear regression analysis, Spearman's rho (SR) test,

the Theil–Sen approach (TSA), Sen's slope, innovative trend analysis (ITA) and the moving trend method (MTM) [28–36]. The climate variability and its trends can be assessed through parametric (*t*-test, F-test, linear regression) and non-parametric (Mann–Kendall test, Sen's slope estimator) methods. The application of parametric methods is constrained to time series that follow a normal distribution. The climate time series, specifically precipitation, do not meet the normality requirement and thus the non-parametric method is applied for trend analysis [37], which has been followed in this study. In the case of data with outliers, non-parametric methods are deemed more robust than parametric methods [38]. Although a traditional method, the Mann–Kendall (MK) test, is the most widely utilised approach, the use of this method is constrained by assumptions such as the serial independence of time series data [39] and the inability to analyse trend behaviours across different categories (low, medium and high) of time series [40,41]. The MMK test is an enhancement of the traditional Mann–Kendall test, which offers a statistically rigorous approach to trend the detection of data with autocorrelation [42]. ITA provides visual inspection and allows for the categorisation of trends and is suitable for comprehensive trend analysis [40].

In Australia, the frequency and volume of rainfall are the primary constraining factors in water security levels [43]. There are limitations in the monitoring and reporting of water quality in regional towns. Wyrwoll et al. [44] have reported that there is limited water quality parameter testing and reporting in 24 local councils. The data and reports are inconsistent and do not comply with the Australian Water Quality Guidelines. Furthermore, Queensland government regulations do not require water utilities to furnish thorough quantitative data analysis and reporting for each parameter [7]. Thus, there is a necessity to gain a deep understanding of both the quantitative and qualitative aspects of rainfall and water quality variations, offering a detailed understanding for water quality management. Moreover, the study covering small scale catchments can minimise natural and anthropogenic variability that may evade the impacts of averaging across larger areas [45]. There is a lack of research on the observation of combined trends and correlation of rainfall and water quality. Therefore, a multi method approach of trend and correlation analysis can provide a holistic understanding of the shifts of hydrological and environmental variables.

The aim of this study is to examine the trends of rainfall and water quality parameters and to explore the correlation between the signals of precipitation and water quality parameters. This analysis was carried out for three water supply reservoirs (Cooby, Cressbrook and Perseverance) in the Toowoomba region of Australia. In this study, two trend analysis methods, namely the modified Mann–Kendall (MMK) test and innovative trend analysis (ITA), were applied for rainfall and water quality trend analyses, respectively. Previously, the water quality index (WQI) was calculated based on five water quality parameters—pH, turbidity, phosphate (PO_4^{3-}), ammonia nitrogen (NH_3-N) and total dissolved solids (TDS) [7]—which have been correlated in this study with rainfall patterns through investigation using the wavelet transform coherence (WTC) method. The explanation and reasons behind the selection of five parameters are elaborated on in our previous study [7]. In summary, the specific objectives are as follows:

- To identify the seasonal trend of rainfall and water quality parameters using a modified Mann–Kendall test (MMK) and innovative trend analysis (ITA), respectively, and to show the spatial distribution of rainfall trend parameters.
- To detect the temporal patterns and correlation between rainfall and water quality index (WQI) using wavelet transform coherence (WTC) spanning a period of 22 years.

2. Materials and Methods

2.1. Study Area

The Toowoomba region is situated in the Darling Downs, Queensland, Australia [46], at an elevation ranging from 125 m to 740 m with an average of approximately 450 m above mean sea level (MSL) [47]. The study area is located in part of the mountain chain that forms the Great Dividing Range of eastern Australia [48]. The average annual rainfall of this region is 735 mm, which peaks in the warm season [49]. The average annual temperature is

19°, while the average summer temperature is 25 °C, and the average winter temperature is 12 °C. Average temperatures across the region are currently 1 °C higher than they were 100 years ago [50]. Three water supply reservoirs, namely Cooby (27.3825° S, 151.9244° E), Cressbrook (27.2641° S, 152.1959° E) and Perseverance (27.2883° S, 152.1239° E), serve as the main source of water supply in this region. The water supply capacity of the three reservoirs is 19.7 megalitres (ML), 78.8 megalitres (ML) and 26.9 megalitres (ML), respectively, and the storage area is 306 ha, 517 ha and 250 ha, respectively. The total catchment area of Cressbrook, including Perseverance reservoir, is 320 km^2 and that of the Cooby catchment is 159 km^2 [51]. The catchments are situated in a warm/humid climatic zone of subtropical Australia, featuring distinctly cool, dry winters and warmer, wetter summers [7]. The topography of the catchments features gentle slopes at lower elevations and hills at higher elevations [48]. Twelve rainfall stations surrounding the three dam reservoir catchments were considered in order to observe the trends of rainfall within this region. The selected rainfall stations and water supply reservoirs are illustrated in Figure 1.

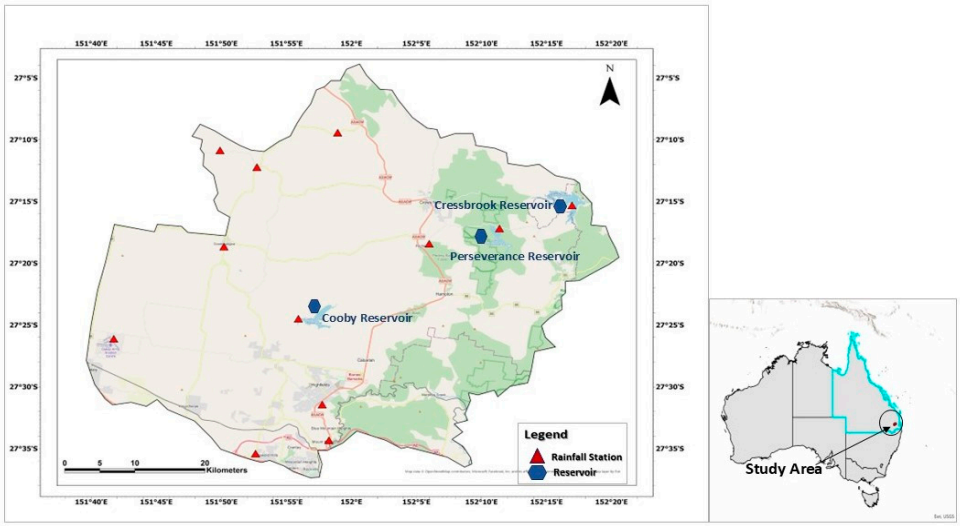

Figure 1. Study area map. The left map shows the area of rainfall stations, including the location of Cooby, Cressbrook and Perseverance reservoirs. The right map is the map of Australia, in which the blue highlighted area is the state of Queensland and the red marks indicate the approximate location of reservoirs.

2.2. Data Collection and Compilation

The water quality data of three dam reservoirs were collected from the Toowoomba Regional Council (TRC), which is responsible for the management of the dam reservoirs and potable water supply in the Toowoomba region. Twenty-two years (2001–2022) of weekly water quality data were collected from TRC. Five water quality parameters affected by rainfall runoff, such as pH, turbidity, total dissolved solids (TDS), ammonia nitrogen (NH_3-N) and phosphate (PO_4^{3-}), were considered for computing the Water Quality Index (WQI) [7]. In conjunction with the water quality data collection, daily rainfall data were collected over the same time span from the Bureau of Meteorology (BOM), Australia (http://www.bom.gov.au/, accessed on 7 March 2024).

There are four seasons in Australia (summer, autumn, winter, and spring) [52]. The summer season includes the three hottest months December, January and February and the winter season includes the three coldest months June, July and August. The trends of water quality parameters and rainfall were scrutinised across four seasons throughout the timeframe (2001–2022) using the modified Mann–Kendall (MMK) test and the innovative trend analysis (ITA) method. The combined use of these two methods provided a comprehensive understanding of seasonal trends (both monotonic and nonmonotonic) of rainfall and water quality. The dataset was checked, and missing values were handled

appropriately. Additionally, wavelet transform coherence (WTC) was utilised to examine the correlation between rainfall and WQI. The trend analysis and wavelet transform were conducted using R 4.3.2 software, and the spatial distribution of rainfall was analysed in ArcGIS Pro software v3.03. The applied techniques are described in the following sections, with the flow diagram showing the research method (Figure 2).

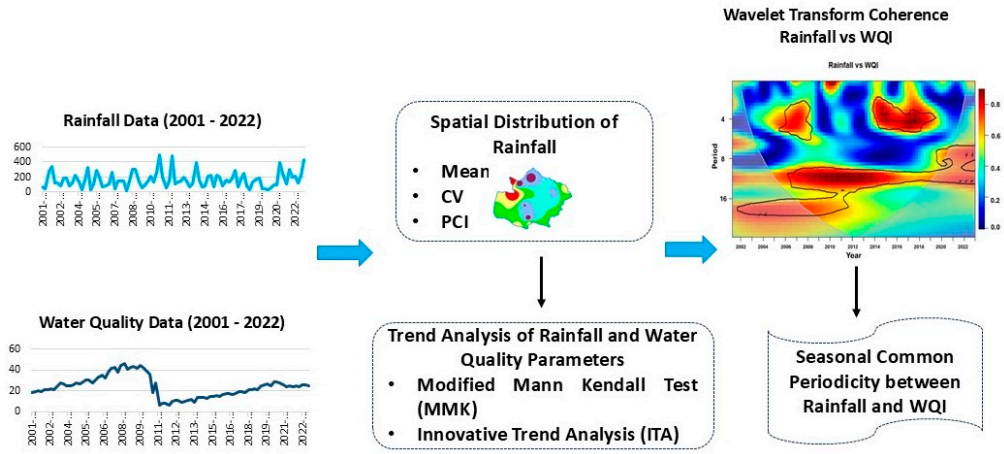

Figure 2. The schematic framework of the research method.

2.3. Precipitation Concentration Index (PCI)

The term precipitation concentration index (PCI) was proposed by Oliver [53] to enumerate the temporal variability of rainfall, also used in soil erosion studies [54]. This index, generally applied on annual scales, represents the monthly precipitation and precipitation heterogeneity within a year. A value between 8.3 and 10 indicates uniform distribution, with a moderate level of uniformity in the distribution of precipitation falling in the range from 10 to 15, and values from 15 to 20 indicating an irregular distribution of precipitation. A value greater than 20 characterises a strong concentration of irregular precipitation over a limited period [53]. In this study, the PCI values were calculated using Equation (1) in Table 1 to examine the spatial and temporal variability of precipitation applied to monthly precipitation [1] data from 2001 to 2022.

2.4. Coefficient of Variance (CV)

The coefficient of variance (CV) or normalised root mean square deviation is a relative measurement of deviation of frequency distribution. It is calculated by dividing the standard deviation of a series by the mean of the series [55]. The formula to calculate CV (Equation (2)) is provided in Table 1. The degree of variability of rainfall is classified by the coefficient of variation (CV) [56]. The rainfall events' variability is classified as high (CV > 30), moderate (20 < CV < 30) or low (CV < 20) [56]. CV was computed in this study to assess the relative annual variability of rainfall in the region.

2.5. Mann–Kendall (MK) and Modified Mann–Kendall (MMK) Tests

The Mann–Kendall (MK) test is a non-parametric statistical test applied to determine the monotonic upward and downward trend in time series data [57]. This test exhibits upward and downward trends with statistical significance [58]. The MK statistics increase by one if the data point of a year is greater than the preceding year and, if the converse occurs, it decreases by one. This test performs well if there is no autocorrelation in the data. This test provides a test variable (S) and a variance (Equations (3) and (4)) in Table 1.

The monotonic trend in the time series can be determined by the Z value. The positive value indicates an increasing trend, whereas the negative value suggests a decreasing trend. The statistical significance of the trend is determined by the specific *p*-value, with a value less than 0.05 indicating statistical significance [59].

The use of the MK method is constrained by autocorrelation effects in data. If there is autocorrelation in the time series, the MK method may indicate a trend if no actual trend exists [42]. A sequential Mann–Kendall test is used to define the starting time of a significant trend in time series [60]. Whereas, in the MMK test, the modified VAR(S) is applied to detect the trend, as shown in Equation (5) (Table 1). In this study, the MMK test was applied to assess the seasonal trends of both rainfall and water quality parameters. The significance of a trend was determined based on a *p*-value. The trend with a *p*-value less than 0.05, which corresponds 5 percent uncertainties or less, was considered to be a significant trend.

2.6. Sen's Slope Estimator

The magnitude of the trend slope is estimated by a non-parametric procedure known as Sen's slope estimator [61]. The equation of Sen's slope (Equation (6)) is provided in Table 1. In this study, Sen's slope estimator was used to quantify the amount of change in a season per year.

2.7. Innovative Trend Analysis (ITA)

The innovative trend analysis (ITA) is a non-parametric graphical method first introduced by Şen [62]. This method is capable of handling autocorrelation and outliers within time series data, detecting both monotonic trends and sub-trends, and identifying combinations of trends across different periods [63]. In the ITA method, firstly the times series is divided into two sub-series each containing an equal number of observations. Subsequently, both series are sorted in ascending order and plotted against each other in a Cartesian coordinate system. In the plot, the first half is plotted on the X axis while the second half is plotted on the Y axis. In the later phase, a straight line is fitted in the scatter plot, which displays either a monotonic trend or no trend. If most scattered points lie above the 1:1 (45°) line, there is an increasing trend in the time series; conversely, if the points cluster below the 1:1 line, this indicates a decreasing trend. Similarly, no trend is signified in the data series, if the points clustered along the trend line [62]. A trend detector was used to examine whether the trend was increasing or decreasing (Equation (7) in Table 1). The ITA method calculations were performed on both rainfall and water quality data series. The innovative trend detection (ITD) was shown as increasing or decreasing using up arrows or down arrows, respectively. Another approach, innovative polygon trend analysis (IPTA) has also been proposed by Şen et al. [64]. This can identify the trend in a particular sequence by providing a trend polygon for the linguistic and numerical interpretation of trends. However, we applied the ITA method in this study to easily identify straightforward trends and shifts rather than using complex visualisation techniques.

2.8. Wavelet Analysis

Wavelet analysis is a dominant analytical tool for analysing processes exhibiting a time–frequency representation of signal in the time domain [65]. Wavelet transform provides localised frequency decomposition, offering insights into frequency components, and, as a consequence, wavelets have a notable dominance over Fourier analysis [66]. In this study, continuous wavelet tools, particularly wavelet coherence, were applied to measure and examine the degree of local correlation between two time series of rainfall and water quality indices in the time–frequency domain, along with wavelet coherence phase differences. The fundamental concepts of wavelet and wavelet transform coherence are explained in the following sections.

2.8.1. Wavelet

A wavelet can be defined as per [66]. It is a true valued square integrable function and can be interpreted as illustrated in Equation (8) (Table 1). A wavelet consists of two control parameters, location, and scale parameter. The location parameter (u) determines the precise position of the wavelet, whereas the scale parameter(s) defines the extent of the

expansion of the wavelet. Scale is inversely related to frequency; therefore, a lower scale means a more compressed wavelet, and a higher scale means a less compressed wavelet. A more compressed wavelet can detect higher frequencies of a time series [66].

2.8.2. Wavelet Transform Coherence (WTC)

A bivariate framework known as wavelet coherence explores the interaction between two time series. Wavelet transform coherence (WTC) locates the sections in the time–frequency space where two distinct time series are certainly not powerful. The wavelet coherence of the time series is calculated by using Equation (9) in Table 1. The value of the squared wavelet coherence coefficient (R_n in Equation (9)) represents the correlation [66]. Values close to 1 indicate a strong correlation whereas values close to 0 exhibit a weak correlation. Thus, the squared wavelet coherence estimates the local linear correlation between two time series that is homogeneous to the squared correlation coefficient in linear regression [66]. The equations of the proper smoothing operator (S) for Morlet wavelet coherence are provided in Table 1 (Equations (10)–(12)). For the Morlet wavelet, a factor of 0.6 is experimentally designated as the scale decorrelation length [67–69].

In wavelet coherence plots, the thick black contour represents the 5% significance level. The cone of influence (COI) is the region in the plot where the edge affects the wavelet power (lighter shading in the plot) and the phase is indicated by arrows. Zero phase difference means the analysed time series move together. Arrows pointing to the right indicate in-phase, while those pointing to the left indicate anti-phase. Arrows pointing up indicate that the first time series leads the second one by 90° and arrows pointing down indicate that the second one is leading the first time series. The stronger correlation is displayed as red and yellow colours in the plot and the blue colour specifies a weak correlation. In the present study, a combination of arrows pointing in different directions was observed in the plot.

Table 1. List of equations used in the analysis.

Equation	SN.	Descriptions	References
$PCI_{annual} = \frac{\sum_{i=1}^{12} Ri^2}{\left(\sum_{i=1}^{12} Ri\right)^2} \times 100$	(1)	PCI = Precipitation concentration index R_i = Rainfall in month i.	[54]
$CV = \frac{\sigma}{\mu}$	(2)	σ = Standard deviation μ = Mean of the series	[55]
$S = \sum_{i=1}^{n-1} \sum_{j=i+1}^{n} sign(X_j - X_i)$	(3)	n = Number of data; X_i, X_j = data points of time series i and j	[58]
$VAR(S) = \frac{1}{18}\{(n(n-1)(2n+5) - \sum_{k=1}^{m} t_k(t_k - 1)(2t_k + 5))\}$	(4)	N = Number of data points m = Number of tied groups t_k = Number of ties in kth group	[58]
$VAR(S) = \left(\frac{n(n-1)(2n+5)}{18}\right).\left(\frac{n}{n_e^*}\right)$	(5)	$\frac{n}{n_e^*}$ = Correction factor to adjust the auto correlated data	[42]
$Q_i = \frac{x_j - x_k}{j - k}$	(6)	x_j, x_k = Values of data at time j and k (j > k) i = 1, 2, 3. . .N	[61]
$B = \frac{1}{n} \sum_{i=1}^{n} \frac{10\,(x_j - x_k)}{\bar{x}}$	(7)	B = Trend detector n = Size of individual sub series x_j, x_k = The values of sub series $\bar{x}$ = Average of first sub series x_k.	[62]
$\psi_{u,s}(t) = \frac{1}{\sqrt{s}}\,\varphi\left(\frac{t-u}{s}\right)$	(8)	$1/\sqrt{s}$ = A normalisation factor ensuring the unit variance of the wavelet, with $\|\|\psi_{u,s}\|\|2 = 1$ u = Location parameter s = Scale parameter	[66]
$R_n^2(u,s) = \frac{\left\|S\left(S^{-1}W_n^{XY}(u,s)\right)\right\|^2}{S\left(S^{-1}\|W_n^x(u,s)\|^2\right) S\left(S^{-1}\|W_n^y(u,s)\|^2\right)}$	(9)	R_n = Squared wavelet coherence coefficient ranging from 0 to 1 n = Time index S = Smoothing operator	[65,66]

Table 1. *Cont.*

Equation	SN.	Descriptions	References
$S(W) = S_{scale}(S_{time}(W_n(S)))$	(10)	S_{scale} = Smoothing along wavelet scale S_{time} = Time parameter	[65,66]
$S_{time}(W)\left\| S = \left(W_n(S) \cdot S_1^{\frac{-1^2}{2s^2}}\right)\right\| S$	(11)	S_{time} = Time parameter	[65,66]
$S_{time}(W)\| S = (W_n(S) \cdot C_2 \Pi(0.65))\|$	(12)	C_2 = Normalisation factor, and Π = rectangle function	[65,66]

In this study, the MMK and ITA tests were applied to rigorously detect trends in rainfall and water quality. The MMK test was chosen for its robustness in identifying statistically significant trends while accounting for serial correlation and seasonality, making it ideal for environmental data with autocorrelation. Meanwhile, the ITA was utilised for its visual and intuitive approach. Additionally, WTC was employed to examine the correlation between rainfall and water quality, capturing the time and frequency dimensions of their relationship.

3. Results and Discussion

3.1. Rainfall Distribution

The basic annual rainfall statistics, such as mean, standard deviation (SD), coefficient of variation (CV) and precipitation concentration index (PCI), of 12 rainfall stations around the three dam catchments were analysed from 2001 to 2022. The mean of the long-term annual rainfall varied from 575 mm to 890 mm. The range of SD and CV was 171 mm to 350 mm and 28% to 39%, respectively. The highest mean rainfall was found at Mount Kynoch station, where SD and CV values were also at the highest levels. As discussed in Section 2.4, CV (%) greater than 30 was classified as high variability and between 20 to 30 was classified as moderate variability of rainfall. We found that the value of CV (%) was greater than 30 in 8 rainfall stations, which indicated high variability of rainfall, and the data from the rest four stations could be classified as moderate to highly variable. The PCI value ranged from 15–20, except for Pechey Forestry, which was 14.2 indicating an irregular distribution of precipitation in the region. The findings are presented in Table 2.

Table 2. Summary statistics of annual rainfall of 12 rainfall stations (2001–2022).

Stations	Location		MSL (m)	Annual Rainfall			
	Latitude (°)	Longitude (°)		Mean (mm)	SD (mm)	CV (%)	PCI
Cooby Creek	−27.3825	151.9244	497	648	193	29.8	15.9
Cressbrook Dam	−27.2641	152.1959	295	765	247	32.3	15.8
Doctors Creek	−27.2067	151.8467	612	665	196	29.5	15.2
Glenaven	−27.1882	151.9634	612	709	226	31.9	15.7
Goombungee PO	−27.3072	151.8506	497	600	192	32.0	16.1
Haden PO	−27.2242	151.8833	640	597	198	33.2	17.7
Moyola	−27.5233	151.8819	559	645	222	34.4	16.0
Mount Kynoch	−27.5094	151.9547	739	890	350	39.3	16.2
Oakey Aero	−27.4034	151.7413	406	575	171	29.7	15.9
Pechey Forestry	−27.3042	152.0542	667	763	261	34.2	14.2
Perseverance Dam	−27.2883	152.1239	470	776	221	28.5	15.5
Tamba	−27.4722	151.9481	642	878	314	35.8	15.1

The inverse distance weighting (IDW) method was applied to show the spatial distribution of rainfall in this study. The spatial distribution of mean, CV and PCI is illustrated in Figure 3. The mean rainfall varied from 813 to 890 mm in the stations near the dam catchment area. The value of CV was high (39%) in Mount Kynoch and low (28–30%)

in Oakey Aero, Perseverance Dam and Cooby Creek. The PCI value was in the range of 14–15 (moderate) in the northeast side of the study area and from 15.1–18 (irregular) on the other side.

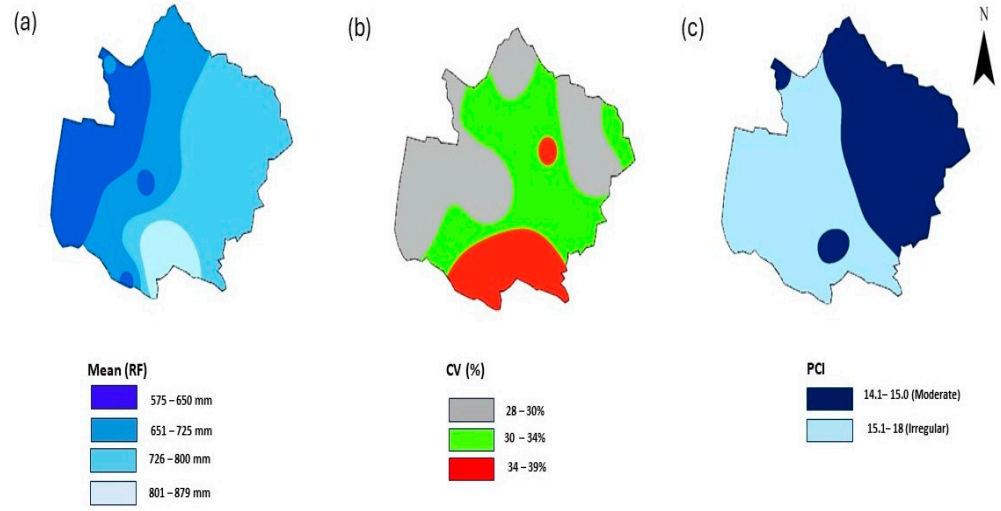

Figure 3. Spatial distribution of rainfall: (**a**) mean (RF), (**b**) coefficient of variation (CV) (%), and (**c**) precipitation concentration index (PCI).

3.2. Auto Correlation Function (ACF)

Table 3 presents the values and plot of lag 1 autocorrelation in seasonal rainfall data for 22 years (2000–2022). In detecting the trend in time series data, the calculation of autocorrelation is a primary step, the magnitude of sequential correlation increases with the variance of the MK test statistic. If there is a positive sequential correlation in the time series data, this amplifies the likelihood of type I errors (false positives) and identifies a noteworthy trend even if there is no genuine trend [70]. In this study, a lag 1 autocorrelation coefficient was calculated at a 95% significance level which was 0.4. It is found that the autumn season rainfall data of Doctors Creek shows autocorrelation at a 95% significance level (highlighted in Table 3). Because autocorrelation exists in the data series in one station, the modified Mann–Kendall (MMK) test was applied to detect the trend of seasonal rainfall.

Table 3. Lag 1 autocorrelation of seasonal rainfall over the years (2001–2022) (yellow highlight indicates that an autocorrelation exists in the data series).

Station	Lag 1 ACF Autumn	Lag 1 ACF Winter	Lag 1 ACF Spring	Lag 1 ACF Summer
Cooby Creek	0.04	−0.06	−0.21	−0.14
Cressbrook Dam	0.34	0.04	−0.29	−0.18
Doctors Creek	0.40	−0.02	−0.25	−0.02
Glenaven	0.23	−0.04	−0.24	0.14
Goombungee PO	0.26	−0.18	−0.30	0.09
Haden PO	0.21	0.16	−0.06	0.11
Moyola	−0.02	−0.01	−0.01	0.05
Mount Kynoch	0.18	0.04	−0.01	0.13
Oakey Aero	0.25	0.08	−0.32	0.28
Pechey Forestry	0.33	−0.05	−0.11	0.23
Perseverance Dam	0.23	0.08	−0.22	−0.35
Tamba	0.28	0.01	−0.10	0.11

3.3. Seasonal Rainfall Trends

3.3.1. Autumn Trend

In scrutinising the trend of rainfall in the autumn season for the entire period of 2001–2022, distinct patterns and fluctuations in precipitation are revealed (Table 4). The Z

values showed increasing rainfall trends in all stations, varying between 0.75 to 2.26 and the maximum is at Cooby Creek station. The trend was significant in Cooby Creek and Moyola stations ($p < 0.05$).

Similarly, the ITA method showed an increasing trend. The indicator values of ITA varied from 1.55–7.38, with the highest at Perseverance Dam (7.38). The detection of the trend is shown by using upward or downward arrows (ITD column) for simplicity.

All other coefficients, such as MK tau Sen's slope and ITA indicator, showed increasing trend (Table 4). According to the value of Sen's slope, the highest change of rainfall in this season was 7.86 mm/yr in Mount Kynoch station whereas according to ITA, Perseverance Dam showed the highest significant trend.

Figure 4 shows the spatial distribution of autumn rainfall trend parameters. Similar and consistent patterns were observed across the parameters, with higher values concentrated in the lower region and lower values in the upper region, which suggests that lower areas were more affected in the region.

Table 4. Rainfall trend (autumn).

Station	Z Statistics	MK Tau	*p* Value	Sen's Slope (mm/yr)	ITD	B (ITA)
Cooby Creek	2.26	0.30	0.02	4.89	↑	3.39
Cressbrook Dam	1.00	0.21	0.72	4.77	↑	1.55
Doctors Creek	1.40	0.30	0.16	5.57	↑	3.81
Glenaven	1.50	0.27	0.13	4.29	↑	2.43
Goombungee PO	1.88	0.31	0.07	5.84	↑	4.51
Haden PO	0.75	0.15	0.45	3.56	↑	3.63
Moyola	2.20	0.30	0.03	5.61	↑	4.90
Mount Kynoch	1.79	0.28	0.07	7.86	↑	5.24
Oakey Aero	1.11	0.21	0.27	4.10	↑	3.69
Pechey Forestry	1.31	0.26	0.19	5.32	↑	4.12
Perseverance Dam	1.36	0.25	0.17	6.34	↑	7.38
Tamba	1.69	0.30	0.09	7.03	↑	6.36

N.B: **ITD** = Innovative trend detection. The red arrow indicates an increasing trend. A significant trend is highlighted by the yellow colour, (p value < 0.05).

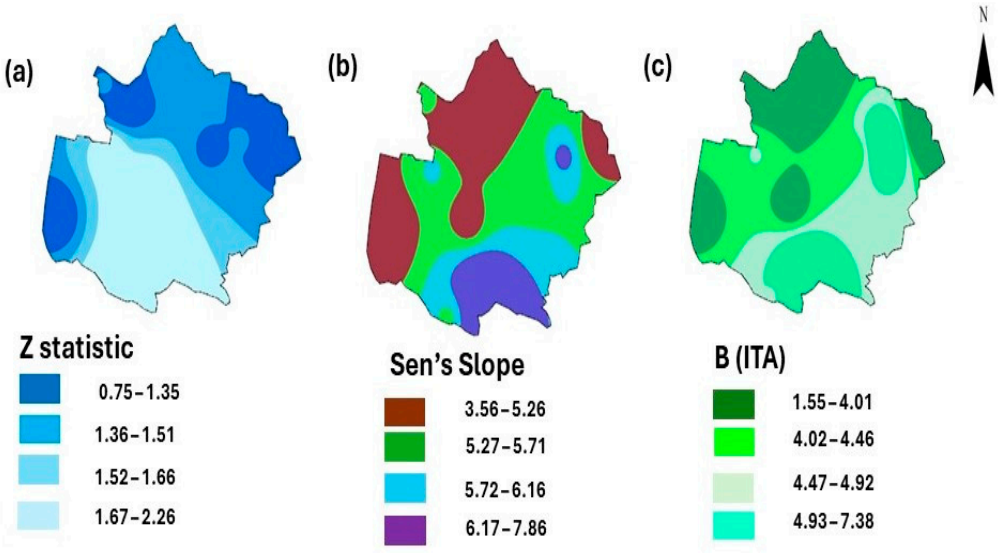

Figure 4. Spatial distribution of autumn rainfall trend parameters. Map (**a**) Z statistics, map (**b**) Sen's Slope, and map (**c**) B (ITA).

3.3.2. Winter Trend

The MMK and ITA methods revealed the same scenarios regarding the winter rainfall trend in the region. Of 12 stations, a non-significant increasing trend was observed in 8 whereas a decreasing trend was found in the remaining 4 stations. The value of Z statistics and ITA indicator were higher at Pechey Forestry, at 0.75 and 0.77 respectively. In Haden PO, the value of Z statistics was minimum (−1.10) indicating a decreasing trend. The average change of rainfall was 0.16 mm/yr. Table 5 illustrates rainfall trends in winter and Figure 5 shows the spatial distribution of winter rainfall trend parameters

Table 5. Rainfall trend (winter).

Station	Z Statistics	MK Tau	*p* Value	Sen's Slope (mm/yr)	ITD	B (ITA)
Cooby Creek	0.50	0.62	0.08	0.75	↑	0.22
Cressbrook Dam	0.36	0.06	0.72	0.53	↑	0.18
Doctors Creek	0.43	0.07	0.67	0.75	↑	0.23
Glenaven	−0.11	−0.02	0.91	−0.24	↓	−0.48
Goombungee PO	0.62	0.08	0.53	0.58	↑	0.20
Haden PO	−1.10	−0.21	0.27	−2.04	↓	−1.82
Moyola	−0.16	−0.03	0.87	−0.42	↓	−0.76
Mount Kynoch	−0.05	−0.01	0.96	−0.27	↓	−0.51
Oakey Aero	0.17	0.03	0.86	0.37	↑	0.23
Pechey Forestry	0.75	0.11	0.45	0.53	↑	0.77
Perseverance Dam	0.39	0.07	0.70	0.52	↑	0.31
Tamba	0.57	0.09	0.57	0.90	↑	0.53

N.B: **ITD** = Innovative trend detection. The red arrow indicates an increasing trend, and the blue arrow shows a decreasing trend.

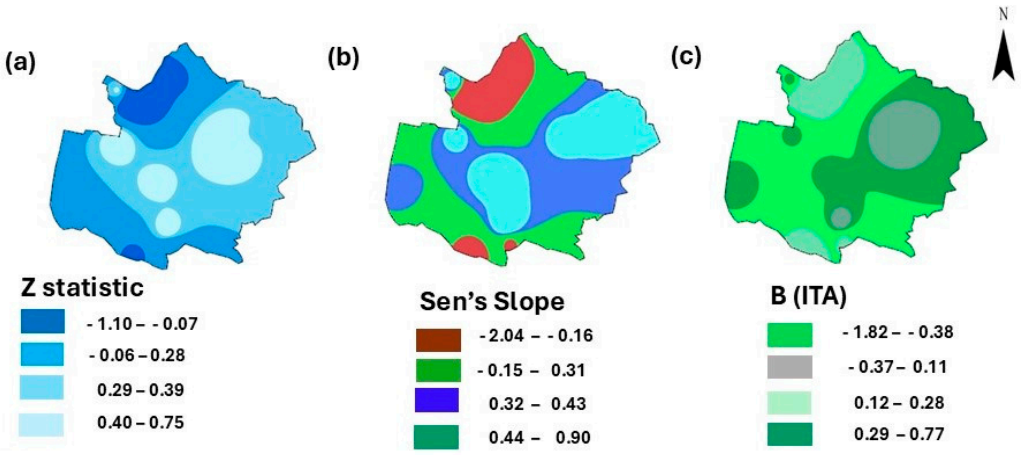

Figure 5. Spatial distribution of Winter rainfall trend parameters. Map (**a**) is Z statistics, Map (**b**) is Sen's Slope, and Map (**c**) is B (ITA).

3.3.3. Spring Trend

The rainfall trend in the spring season was characterised by low rainfall trends. Cooby Creek and Glenaven exhibited negligible trends, with Z statistics close to zero, suggesting stable conditions. Cressbrook Dam, Doctors Creek, Goombungee PO, Moyola, Mount Kynoch, Oakey Aero, and Pechey Forestry implied increasing trends according to the value of Z statistics and ITA indicators. Based on the value of Sen's slope, the average change of rainfall was 0.57 mm/yr. Conversely, Haden PO and Tamba demonstrated negative trends. Additionally, ITA indicator values indicated low-to-moderate variability in precipitation trends. Table 6 illustrates the rainfall trend in the spring season and Figure 6 shows the spatial distribution of spring rainfall trend parameters.

Table 6. Rainfall trend (spring).

Station	Z Statistics	MK Tau	*p* Value	Sen's Slope (mm/yr)	ITD	B (ITA)
Cooby Creek	0.02	0.03	1.00	−0.02	↓	−0.86
Cressbrook Dam	0.28	0.04	0.78	0.47	↓	0.59
Doctors Creek	0.88	0.11	0.38	1.69	↑	0.41
Glenaven	−0.07	−0.01	0.95	−0.20	↓	−0.28
Goombungee PO	0.72	0.08	0.47	2.33	↑	1.45
Haden PO	−0.24	−0.04	0.81	−0.76	↑	−0.99
Moyola	0.32	0.05	0.75	1.51	↑	0.65
Mount Kynoch	0.29	0.05	0.77	1.13	↓	0.56
Oakey Aero	0.22	0.03	0.83	0.57	↑	0.60
Pechey Forestry	0.18	0.03	0.86	0.74	↑	0.75
Perseverance Dam	0.07	0.01	0.95	0.36	↑	0.92
Tamba	−0.06	−0.01	0.95	−0.91	↓	−0.82

N.B: **ITD** = Innovative trend detection. The red arrow indicates an increasing trend, and the blue arrow shows a decreasing trend.

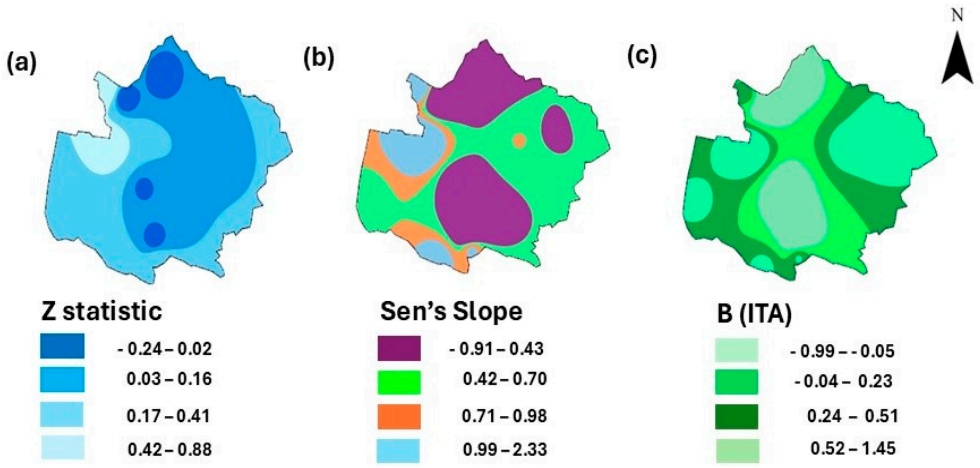

Figure 6. Spatial distribution of spring rainfall trend parameters. Map (**a**) Z statistics, map (**b**) Sen's slope, and map (**c**) B (ITA).

3.3.4. Summer Trend

In examining the summer season's rainfall trend, MMK analysis shows a non-significant increasing trend in seven stations and a decreasing trend in the remaining five stations, as illustrated in Table 7 and Figure 7. Notably, Haden PO stood out, with a negative Sen's slope and Z statistics, indicating a substantial decrease in precipitation. The average change of rainfall in this was 0.13 mm/yr. The value of the ITA indicator varied from −2.11 to 2.25.

Table 7. Rainfall trend (summer).

Station	Z Statistics	MK Tau	*p* Value	Sen's Slope (mm/yr)	ITD	B (ITA)
Cooby Creek	−0.24	−0.04	0.81	−0.89	↓	−0.64
Cressbrook Dam	0.62	0.08	0.53	2.80	↑	0.20
Doctors Creek	0.43	0.07	0.67	2.00	↑	1.48
Glenaven	0.23	0.04	0.82	0.48	↑	0.77
Goombungee PO	−0.10	−0.02	0.92	−0.26	↓	−0.53
Haden PO	−1.46	−0.21	0.14	−5.48	↓	−2.11
Moyola	0.10	0.02	0.92	0.14	↑	0.49

Table 7. *Cont.*

Station	Z Statistics	MK Tau	*p* Value	Sen's Slope (mm/yr)	ITD	B (ITA)
Mount Kynoch	0.47	0.08	0.64	3.31	↑	2.25
Oakey Aero	−0.42	−0.05	0.68	−1.40	↓	−0.77
Pechey Forestry	−0.30	−0.06	0.77	−1.71	↓	−0.75
Perseverance Dam	0.53	0.06	0.60	0.87	↑	0.24
Tamba	0.52	0.09	0.60	1.73	↑	0.10

N.B: **ITD** = Innovative trend detection. The red arrow indicates an increasing trend, and the blue arrow shows a decreasing trend.

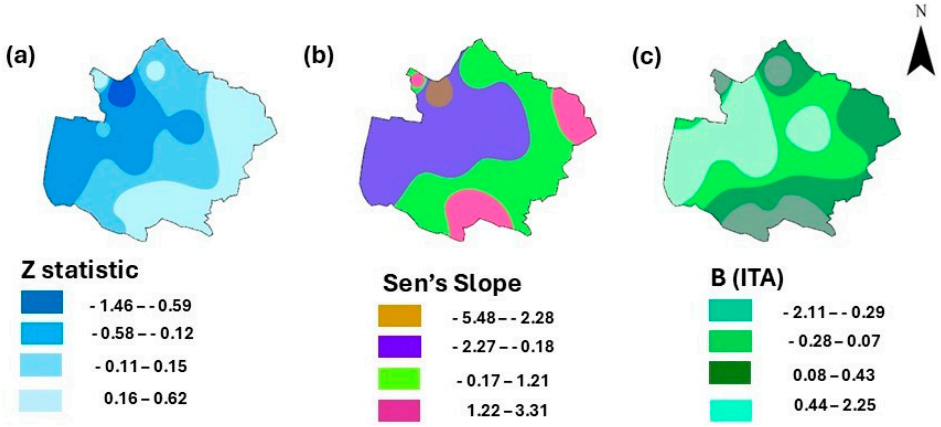

Figure 7. Spatial distribution of summer rainfall trend parameters. Map (**a**) Z statistics, map (**b**) Sen's slope, and map (**c**) B (ITA).

3.4. Trend of Seasonal Water Quality

The aim of this analysis was to elucidate temporal variations in water quality across four distinct seasons spanning 22 years (2001–2022). This comprehensive study examined trends in five water quality parameters—ammonia nitrogen (NH_3-N), pH, phosphate (PO_4^{3-}), total dissolved solids (TDS), and turbidity along—with the water quality index (WQI), which was determined based on these five parameters. The selection of parameters, computation of WQI, and its analysis are discussed in detail in a previous study [7]. The WQI trends detected by the MMK and ITA method. The findings are illustrated in the following sections.

3.4.1. Cooby Reservoir

The trend results of both MMK and ITA provided a combination of both increasing and decreasing trend of water quality parameters. Out of five water quality parameters, only PO_4^{3-} exhibited a significant decreasing trend in all four seasons. There was no change in the concentration based on the value of Sen's slope. The trend of NH_3-N was non-significantly increasing, pH showed an increasing trend in winter and spring and a decreasing trend in autumn and summer. The TDS showed almost no trend in winter but an increasing trend in the other seasons. The turbidity of water exhibited a non-significant increasing trend in all four seasons.

As shown in Table 8 and the WQI of this reservoir exhibited a decreasing trend in all four seasons. The average change was −1.74 according to the value of the ITA indicator. In WQI calculation [7], the maximum weightage (5 on a scale of 1–5) was assigned to NH_3-N and PO_4^{3-}, and the minimum weightage 3 was assigned to turbidity. Both TDS and pH had a weightage of 4. The relative effects were observed with WQI trend, with an increasing trend of NH_3-N, TDS and pH in autumn and summer, resulting in an overall decreasing trend of WQI. Hence, the effects of the decreasing trend of PO_4^{3-} might not have much impact on the WQI trend. The ITA plots of Cooby reservoir is shown in Figure 8.

Table 8. Details of water quality parameters trend (Cooby reservoir).

Parameter	Season	Z Statistic	MK Tau	*p* Value	Sen's Slope	ITD	B (ITA)
NH_3-N	Autumn	0.33	0.12	0.74	0.01	↑	0.07
	Winter	0.35	0.13	0.73	0.01	↑	2.37
	Spring	0.50	0.11	0.62	0.01	↑	0.27
	Summer	0.08	0.03	0.94	0.01	↑	0.30
pH	Autumn	−0.25	−0.04	0.81	0.00	↓	−0.06
	Winter	0.84	0.11	0.40	0.01	↑	0.00
	Spring	0.61	0.09	0.54	0.00	↑	0.08
	Summer	−1.33	−0.19	0.18	−0.01	↓	−0.10
PO_4^{3-}	Autumn	−3.19	−0.39	0.00	0.00	↓	−4.10
	Winter	−2.09	−0.38	0.04	0.00	↓	−3.83
	Spring	−4.55	−0.64	0.00	0.00	↓	−3.95
	Summer	−4.22	−0.63	0.00	0.00	↓	−4.30
TDS	Autumn	0.06	0.03	0.95	2.64	↑	1.89
	Winter	0.00	0.00	1.00	0.73	↑	1.93
	Spring	0.04	0.02	0.97	2.55	↑	1.81
	Summer	0.13	0.05	0.90	2.49	↑	1.81
Turbidity	Autumn	1.24	0.18	0.21	0.04	↑	0.09
	Winter	0.87	0.15	0.38	0.03	↑	0.03
	Spring	0.42	0.14	0.68	0.02	↑	0.95
	Summer	0.20	0.04	0.84	0.01	↓	0.09
WQI	Autumn	−0.06	−0.03	0.95	−0.15	↓	−1.83
	Winter	−0.04	−0.02	0.97	−0.05	↑	−1.82
	Spring	−0.06	−0.03	0.95	−0.05	↓	−1.60
	Summer	−0.04	−0.02	0.97	−0.03	↓	−1.73

N.B: **ITD** = Innovative trend detection. The red arrow indicates the increasing trend, and the blue arrow shows the decreasing trend. A significant trend is highlighted with the yellow colour (p value < 0.05).

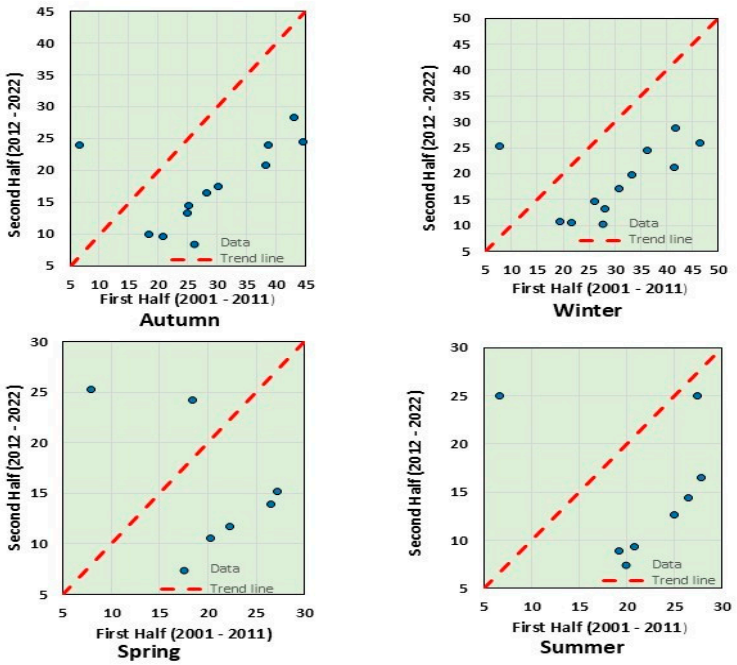

Figure 8. Plot of the innovative trend of WQI time series of Cooby reservoir (2001–2022). The blue dots represent the WQI in different seasons.

3.4.2. Cressbrook Reservoir

For Cressbrook reservoir, it was observed from MMK and ITA outcomes that NH_3-N had an increasing trend in all seasons (Table 9). pH and turbidity demonstrated a non-significant increasing trend in autumn, winter and summer and a decreasing trend in spring. However, PO_4^{3-} exhibited a significant declining trend entirely in all four seasons, where the minimum Z statistics value was noted in autumn (−4.88). In the case of Cooby, turbidity showed an increasing trend in all seasons, but in Cressbrook, the trend was decreasing in spring season. Like Cooby, TDS showed no trend in winter. Furthermore, WQI showed a non-significant declining trend across all four seasons. There was a slight increase in spring in the second half of the data (2012–2022) (Figure 9). In relation to the WQI of Cooby reservoir, the increasing trend of NH_3-N, turbidity and pH also affected the overall trend of WQI of this reservoir. Based on the value of Sen's slope, the WQI is decreasing by −0.01 on average per year (Table 9).

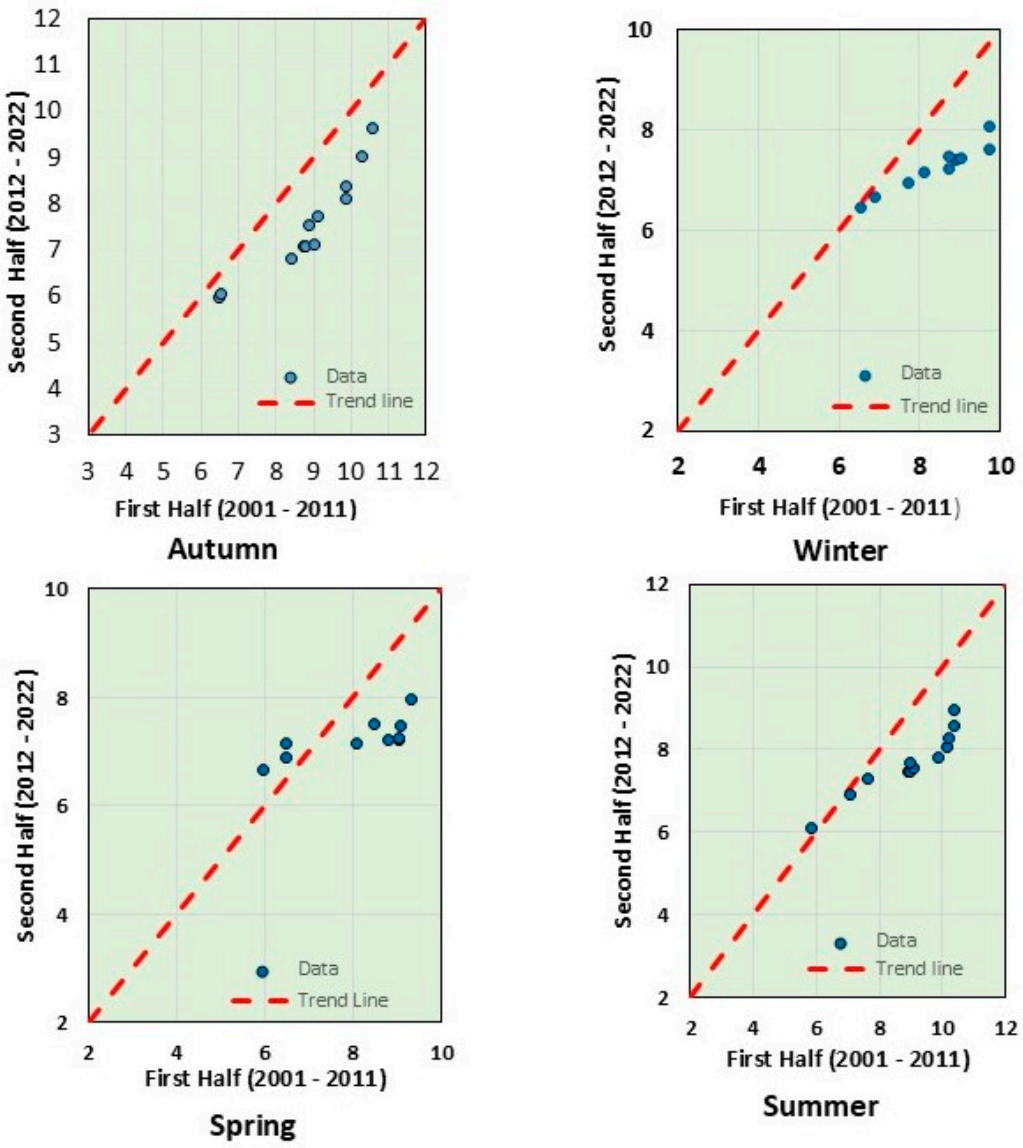

Figure 9. Plot of the innovative trend of the WQI time series of Cressbrook reservoir (2001–2022). The blue dots represent the WQI in different seasons.

Table 9. Details of water quality parameters trend (Cressbrook reservoir).

Parameter	Season	Z Statistic	MK Tau	*p* Value	Sen's Slope	ITD	B (ITA)
NH_3-N	Autumn	0.95	0.16	0.34	0.01	↑	0.06
	Winter	1.73	0.27	0.08	0.01	↑	0.05
	Spring	0.58	0.95	0.56	0.01	↑	0.62
	Summer	0.40	0.11	0.69	0.01	↑	0.06
pH	Autumn	0.22	0.04	0.82	0.00	↑	0.01
	Winter	0.87	0.19	0.38	0.01	↑	0.03
	Spring	−0.25	−0.04	0.81	0.00	↓	−0.09
	Summer	0.19	0.04	0.85	0.00	↑	0.03
PO_4^{3-}	Autumn	−4.88	−0.51	0.00	0.00	↓	−1.06
	Winter	−4.59	−0.52	0.00	0.00	↓	−1.52
	Spring	−3.90	−0.58	0.00	0.00	↓	−1.22
	Summer	−3.55	−0.61	0.00	0.00	↓	−1.31
TDS	Autumn	−0.24	−0.08	0.81	−0.88	↓	−0.98
	Winter	0.00	0.00	1.00	−0.02	↓	−0.08
	Spring	−0.09	−0.04	0.93	−0.46	↓	−0.84
	Summer	−0.16	−0.06	0.88	−0.48	↓	−0.59
Turbidity	Autumn	2.08	0.33	0.04	0.05	↑	0.69
	Winter	1.29	0.19	0.20	0.03	↑	0.33
	Spring	−0.30	−0.08	0.76	−0.01	↓	−0.08
	Summer	0.88	0.20	0.38	0.02	↓	−0.68
WQI	Autumn	−0.05	−0.02	0.96	−0.01	↓	−0.01
	Winter	−0.13	−0.05	0.89	−0.01	↓	−0.71
	Spring	−0.10	−0.04	0.92	−0.01	↓	−0.56
	Summer	−0.12	−0.04	0.91	−0.02	↓	−0.72

N.B: **ITD** = Innovative trend detection. The red arrow indicates the increasing trend and the blue arrow shows the decreasing trend. A significant trend is highlighted with the yellow colour (*p* value < 0.05).

3.4.3. Perseverance Reservoir

A noticeable difference in trend was observed in Perseverance reservoir compared with the other two reservoirs. Most significantly, WQI showed a significant increasing trend in three seasons, except for spring, while the other two exhibited a declining trend. This matched with the pH trend as non-significantly decreasing in summer while increasing in the other three seasons. Similarly, PO_4^{3-} revealed a significant decreasing trend, while TDS showed a significant increasing trend in winter and spring and turbidity was significantly increasing in spring. In comparison with the WQI of the other two reservoirs, the WQI was very poor (<10) in this reservoir [7]. The slight increasing trend was positive for this reservoir water quality and the average increase was 0.06, based on the value of Sen's slope (Table 10). The WQI trends detected by the ITA method is shown in Figures 10 and 11 is the Z statistic plot of the water quality parameters of three reservoirs.

Table 10. Details of water quality parameters trend (Perseverance reservoir).

Parameter	Season	Z Statistic	MK Tau	*p* Value	Sen's Slope	ITD	B (ITA)
NH_3-N	Autumn	0.87	0.22	0.39	0.01	↑	0.53
	Winter	0.38	0.16	0.71	0.00	↑	0.99
	Spring	0.40	0.14	0.69	0.00	↑	0.05
	Summer	0.17	0.08	0.86	0.01	↑	0.05
pH	Autumn	0.10	0.03	0.92	0.00	↑	0.01
	Winter	0.41	0.11	0.68	0.01	↑	0.06
	Spring	0.27	0.05	0.79	0.01	↑	0.08
	Summer	−0.06	−0.02	0.95	0.00	↓	−0.01

Table 10. *Cont.*

Parameter	Season	Z Statistic	MK Tau	*p* Value	Sen's Slope	ITD	B (ITA)
PO_4^{3-}	Autumn	−3.76	−0.54	0.00	−0.01	↓	−1.00
	Winter	−2.33	−0.40	0.02	0.00	↓	−1.25
	Spring	−2.35	−0.51	0.02	0.00	↓	−0.04
	Summer	−2.72	−0.63	0.01	0.00	↓	−0.52
TDS	Autumn	1.61	0.38	0.11	1.43	↑	1.11
	Winter	1.97	0.38	0.05	1.34	↑	1.65
	Spring	2.05	0.44	0.04	1.47	↑	2.01
	Summer	1.77	0.49	0.08	1.60	↑	1.63
Turbidity	Autumn	1.82	0.40	0.07	0.16	↑	0.63
	Winter	2.18	0.33	0.29	0.14	↑	0.89
	Spring	2.14	0.42	0.03	0.16	↑	0.99
	Summer	1.64	0.42	0.10	0.17	↑	0.93
WQI	Autumn	2.05	0.45	0.04	0.06	↑	0.40
	Winter	1.87	0.46	0.06	0.05	↑	0.41
	Spring	1.69	0.42	0.09	0.05	↑	0.33
	Summer	2.13	0.57	0.03	0.07	↑	0.44

N.B: **ITD** = Innovative trend detection. The red arrow indicates the increasing trend, and the blue arrow shows the decreasing trend. A significant trend is highlighted with the yellow colour (p value < 0.05).

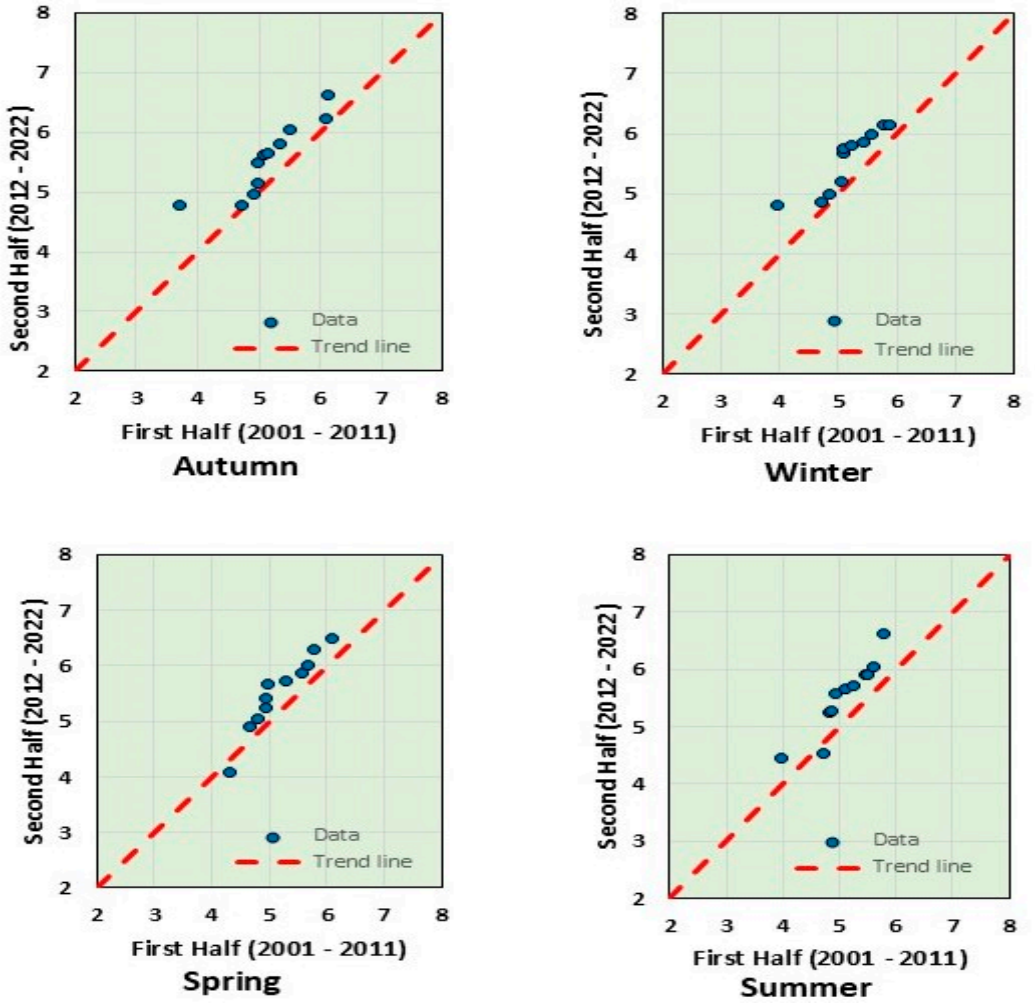

Figure 10. Plot of the innovative trend of WQI time series of Perseverance reservoir (2001–2022). The blue dots represent the WQI in different seasons.

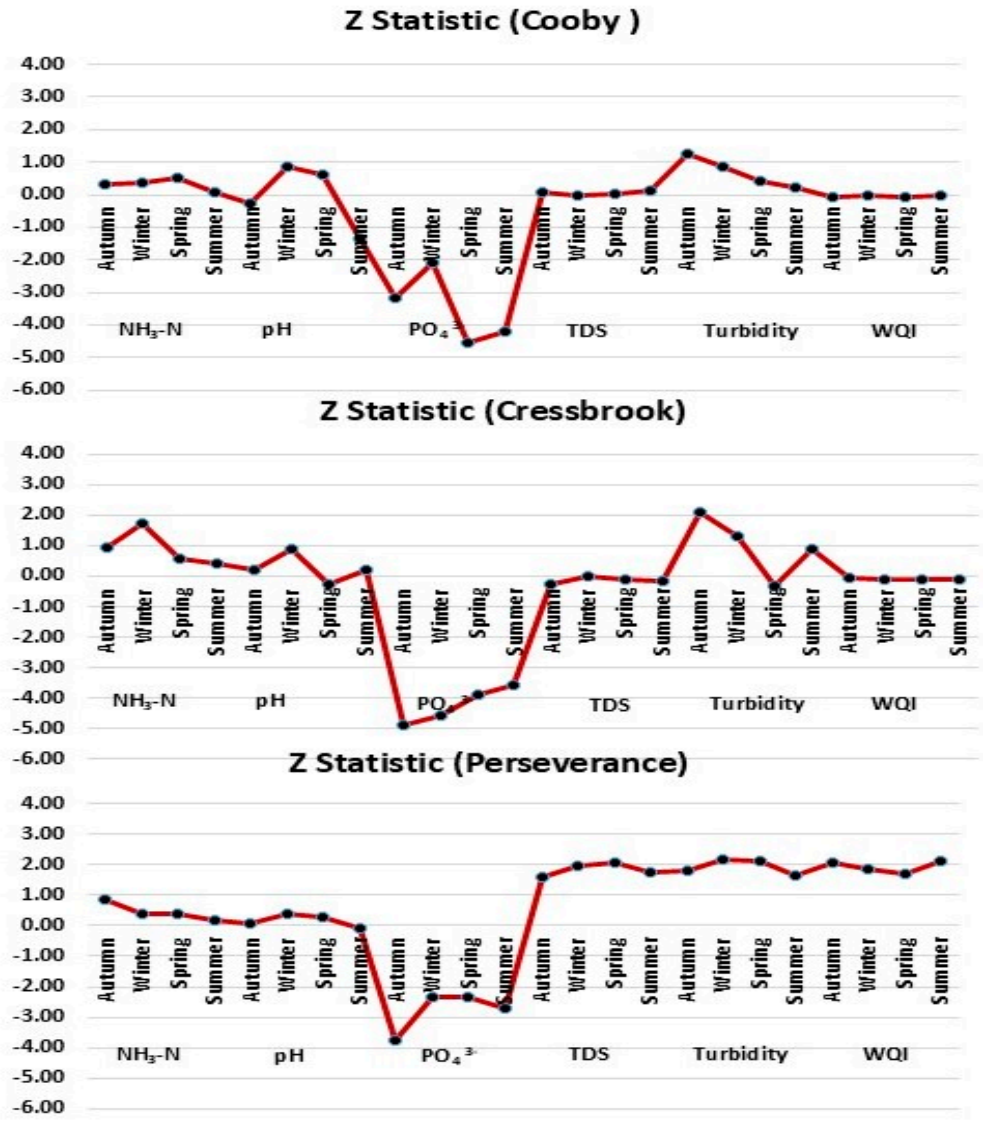

Figure 11. Modified Mann–Kendall test Z statistic plot, (**top**) Cooby, (**middle**) Cressbrook, (**bottom**) Perseverance.

3.5. Comparative Analysis of MMK and ITA Trend Methods

In this study, the observation of the rainfall and water quality data revealed distinct and significant insights into trends through the application of both traditional and statistical method MMK, and the more recent and graphical ITA method.

In terms of identifying the trend of rainfall, the trend detection from both MMK and ITA was mostly consistent. Both methods had identified notable trends where these were present, complementing each other's findings and providing a comprehensive understanding of seasonal rainfall variations. For example, in the autumn season, Cooby Creek and Moyola rainfall stations showed a significant increasing trend in rainfall, with ITA indicators of 3.39 and 4.90 values respectively.

Similarly, in the analysis of water quality trends across the Cooby, Cressbrook and Perseverance reservoirs, both methods demonstrated the same alignment. In all reservoirs, PO_4^{3-} showed a significant decreasing trend in all seasons and the average ITA indicator values were −4.40 in Cooby −1.27 in Cressbrook and −0.70 in Perseverance reservoir. The WQI showed a significant increasing trend in the Perseverance reservoir, which was also matched with the ITA indicator.

Compared with the MMK method, the ITA method offers several distinct advantages. It is more effective in identifying trends, particularly those subtle variations in data that conventional methods such as MMK may overlook. ITA's visual and graphical representation of trends make it easier to identify extreme events such as significant rainfall leading to flooding or minimal rainfall resulting in drought [39]. In this study, the ITA graphs were generated for WQI only, in order to examine how WQI has changed over various seasons during the period of 22 years. These plots clearly show that WQI was on a decreasing trend in the first half (2001–2011) of the time series in Cooby and Cressbrook reservoirs. In this period, Toowoomba region experienced drought from 2000–2006 and extreme flooding from December 2010 to January 2011 [71]. Although the WQI showed a slight increasing trend in Perseverance reservoir, this was noticed in the second half of the data (2012–2022). ITA graphs allowed easy recognition of recurring patterns or periodic fluctuations of WQI. This visual approach can be particularly useful when identifying changes that might be masked by the MMK test.

Therefore, the MMK test's statistical findings of decreasing or increasing trends in specific seasons were mathematically and visually confirmed by the ITA, which displayed corresponding shifts in the data. This dual approach not only validated the results, but also enhanced the interpretability of the data, making the observations accessible and understandable for broader audiences.

3.6. Wavelet Transform Coherence (WTC) Analysis

Following the trend analysis of rainfall and water quality parameters, the WTC method was applied in this study to identify the significant temporal relationship and co-movement of rainfall and WQI data series and to determine the prevailing frequencies or periods. The WTC plots of rainfall of twelve rainfall stations and WQI are presented in Figures 12–14.

3.6.1. WTC of Rainfall and WQI (Cooby Reservoir)

The temporal relationship between rainfall and the WQI of Cooby reservoir is represented in Figure 12. The individual WTC plot of each station can be found in the link of Supplementary Files. The very high coherency (dark red) was visible in 8–16 periods from 2002–2022 between rainfall and WQI in the Cooby Creek rainfall stations and the Haden Post Office rainfall station (Figure 12a,f). This revealed notably strong coherence at extended frequencies, corresponding to cycles with periodicity in 8 to 16 and exceeding 16 within the time frame spanning from 2005 to 2018 in most of the stations. High correlation was significant in all stations during 4 to 8 periods from 2014 to 2020. On the other hand, low coherence is depicted in the Pechey Forestry Rainfall and WQI plot (Figure 12k), here only 2–4 periods from 2014–2018 exhibited high coherence. In the Doctor's Creek WTC plot, a significant region from 2001 to 2008 with 16 periods was apparent, which showed the rainfall anomaly leading to WQI (straight down arrows in 5% significance level in Figure 12c,d). Based on Figure 12i, a significant region from 2004 to 2014 with an 8 to 16 period is evident. Most of the regions with a 5% significance level were scattered in all plots and are relatively small in Figure 12j,k.

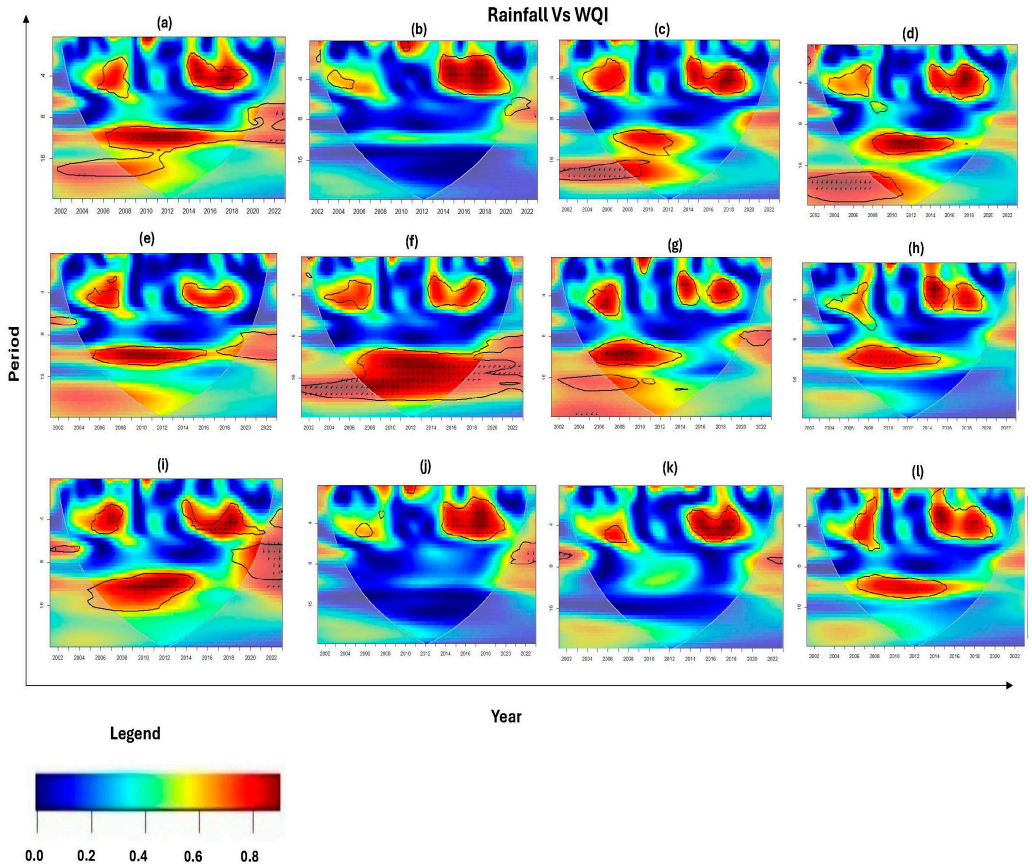

Figure 12. WTC plot of Rainfall and WQI (Cooby). The coherency is shown by colour code, ranging from red (high coherency, value close to 1) to blue (low coherency, value close to 0). Statistically significant periodicity is displayed with black contours indicating a 5% significance level. The time scale 'Year' is shown in x axis and vertical axis (y axis) presents 'Period' across seasons in a year. The twelve rainfall stations are marked with lettering ranging (**a**–**l**). Individual plot of each station is available in the link of Supplementary Files.

3.6.2. WTC of Rainfall and WQI (Cressbrook Reservoir)

WTC plots of rainfall and WQI of Cressbrook reservoir revealed a mid-term overall behaviour of two variables exhibiting a mixed combination of coherency. In all plots of Figure 13, high coherency was displayed from 2015 to 2022 with the period 4 to 16. The arrows are pointing upward and in phase (right). The largest significant region was observed at the Oakey Aero rainfall station (Figure 13i) during the period from 4 to 16, exhibiting a phase status from 2018 to 2022 with a 5% significance level. However, from 2007 to 2012, a significant 8 to 16 period showed an anti-phase status and from 2019 to 2022, with the 8 to 16 period exhibiting a phase status (Figure 13a). Regions with a 5% significant level were scattered across all plots. The individual WTC plot of each station can be found in the link of Supplementary Files.

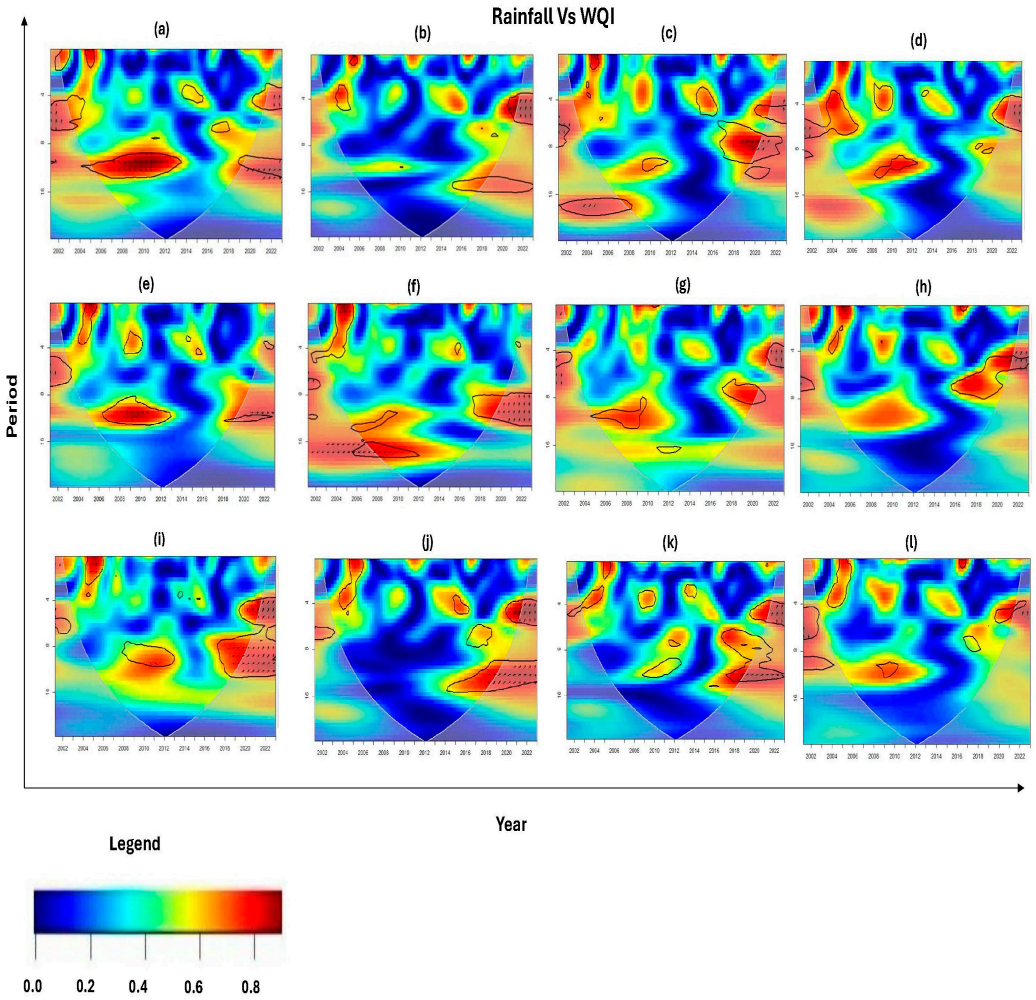

Figure 13. WTC plot of Rainfall and WQI (Cressbrook). The coherency is shown by colour code ranging from red (high coherency, value close to 1) to blue (low coherency, value close to 0). Statistically significant periodicity is displayed with black contours indicating a 5% significance level. The time scale 'Year' is shown in x axis and vertical axis (y axis) presents 'Period' across seasons in a year. The twelve rainfall stations are marked with lettering ranging from (**a**–**l**). Individual plot of each station is available in the link of Supplementary Files.

3.6.3. WTC of Rainfall and WQI (Perseverance Reservoir)

In Figure 14, the WTC is specified for rainfall of twelve stations (a to l) and the WQI for Perseverance reservoir. The individual WTC plot of each station can be found in the link of Supplementary Files. There was a large and significant area in the Haden Post Office plot (Figure 14f) from 2001 to 2016, with 8 to 16 periods that had combinations of upward and downward arrows and other regions with 4 to 8 periods from 2017 to 2020. The 5% significant zones are mostly visible in Oakey Aero (i), Glenaven (d), Tamba (l) and Cooby Creek (a). In the Oakey aero plot, significant coherence was visible in the periods from 2 to 16 between 2018 to 2022 and from 8 to 16 between 2001 to 2012. When comparing the overall coherency of rainfall and WQI across all three reservoirs, relatively low coherence was observed in the case of Perseverance reservoir.

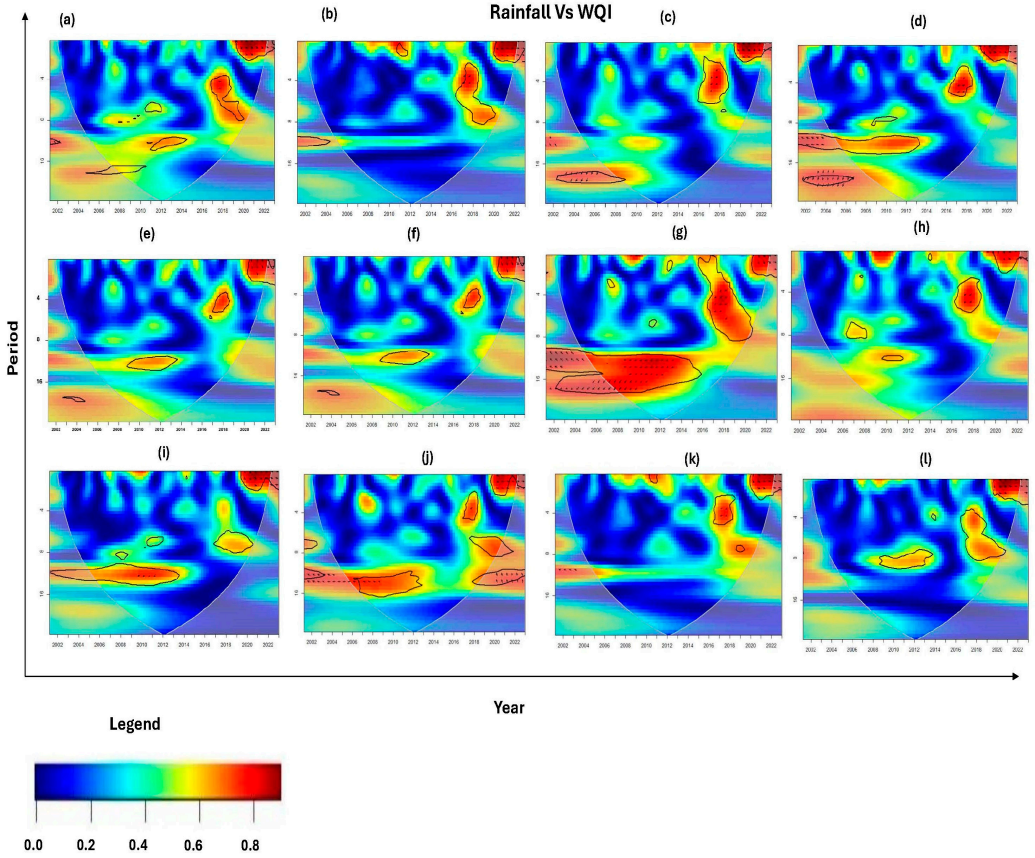

Figure 14. WTC plot of Rainfall and WQI (Perseverance). The coherency is shown by colour code ranging from red (high coherency, value close to 1) to blue (low coherency, value close to 0). Statistically significant periodicity is displayed with black contours indicating a 5% significance level. The time scale 'Year' is shown in x axis and vertical axis (y axis) presents 'Period' across seasons in a year. The twelve rainfall stations are marked with lettering ranging from (**a**–**l**). Individual plot of each station is available in the link of Supplementary Files.

4. Conclusions and Future Works

This study investigated the trend and correlations of rainfall and water quality parameters using statistical, graphical and mathematical methods. Previously, we estimated WQI based on five water quality parameters and this study used statistical trend analysis and applied wavelet transform techniques to demonstrate the pronounced seasonal variation of those parameters and their associated WQI along with rainfall patterns, with the intention of illuminating the complex interactions between climatic factors and water quality dynamics. A thorough exploration of spatial and temporal trends of rainfall and the potential time–frequency relationship between precipitation and water quality variations has been presented. The trends of rainfall across four seasons for the period of 22 years (2001–2022) were investigated using MMK and ITA methods. The MMK test was applied to check if the trend was significant, though the magnitude of the trend was calculated with Sen's slope estimator. The ITA indicator was calculated to observe whether the trend was increasing or decreasing. Both methods (MMK and ITA) were also applied to examine the trend of water quality parameters. In the span of data of 22 years, the MMK test and ITA provided almost the same results in trend analysis. Moreover, wavelet transformation was used to see the correlation between seasonal rainfall and seasonal WQI. The major findings of the study can be summarised as follows:

- A significant increasing trend of rainfall was observed in two rainfall stations (Cooby Creek and Moyola) in autumn and the combination of non-significant increasing and

decreasing trends in the other three seasons. The rainfall during autumn increased by 5.43 mm/yr. The highest value of Sen's slope was also observed in the autumn, (7.86 mm/yr) at Mount Kynoch.

- In water quality trends, NH_3-N showed increasing trends across four seasons in all three reservoirs. PO_4^{3-} showed a significant decreasing trend in all three reservoirs in four seasons and was not affecting the trend of WQI. The declining trend of PO_4^{3-} levels was a positive indicator of improved water quality in the reservoir. It indicated improved agricultural practice reducing phosphate runoff and better environmental regulations aimed at controlling phosphate discharge. The increasing trend of NH_3-N, pH and turbidity affected the overall trend of WQI in Cooby and Cressbrook reservoirs. A slight increasing trend of WQI was observed in the Perseverance reservoir.
- The MMK test provided statistical robustness and identified significant trends in rainfall and water quality data and ITA offered a detailed graphical representation highlighting subtle and nonlinear trends that MMK might have overlooked. In the case of water quality, WQI showed a decreasing trend in the first half of the data (2001–2012) in Cooby and Cressbrook reservoirs and slight increasing trend in the second half of the data in Perseverance reservoir. ITA's visual output was particularly valuable in illustrating gradual changes and potential breakpoints, complementing the statistical validation provided by MMK.
- In wavelet transform coherence (WTC) results, a notable correlation was found between seasonal rainfall and WQI. At Cooby Creek station, a very high coherence was noticed between rainfall and WQI in 8 to 16 periods ranging from 2002 to 2022. The regions with a 5% significance level were scattered in all plots. Among the twelve stations, the higher coherency was visible in Cooby Creek and at the Haden Post Office rainfall station with WQI of all reservoirs. However, comparatively low coherency was observed amidst rainfall and WQI of Perseverance reservoir. In terms of water quality trends and correlation analysis, Perseverance reservoir showed a slightly different scenario. The causes of this difference may include land use practices, catchment size, different outflow and inflow patterns and the variation in distribution and intensity of rainfall. This can be thoroughly investigated in future studies.

A few limitations of this study are worthwhile to mention, MMK relies on more than 30 years of data for optimal outcomes; however, this study utilised 22 years of temporal data, which may affect the overall results. Yang et al. [72] used 20 years of data to observe the changes in water quality and to find the effectiveness of water treatment. The previous studies [32,44] have suggested that both MMK and ITA methods provided reliable results; however, we only considered the rainfall effects due to the availability of data. Future research should explore the impact of runoff on water quality fluctuations.

Overall, this study provided a deeper understanding of the impacts of rainfall variability on water quality fluctuations, capturing both statistically significant changes and visually apparent patterns that provide a clear picture of environmental dynamics, thus informing decision making in water resource management and environmental conservation. Proactive conservation measures and community engagement can be collectively committed towards long-term sustainability and can ensure equitable access to water resources for present and future generations.

Supplementary Materials: The following supporting information can be downloaded at: https://www.mdpi.com/article/10.3390/geosciences14080225/s1.

Author Contributions: Conceptualisation: S.Z.F.; data collection and compilation: S.Z.F.; methods and analysis: S.Z.F.; writing—original draft preparation: S.Z.F.; writing—review and editing: D.R.P., M.J.A. and S.C.; supervision: D.R.P., M.J.A. and S.C. All authors have read and agreed to the published version of the manuscript.

Funding: This research received no external funding.

Data Availability Statement: Data should be available from first author after reasonable request.

Acknowledgments: The authors would like to thank the TRC for providing the water quality data and BOM for rainfall data. This research has been supported by the Graduate Research School, University of Southern Queensland and this is a part of the first author's Ph.D. project entitled "An Integrated Spatial Decision Support Framework for Monitoring and Management of Surface Water Quality Influenced by Climate Change."

Conflicts of Interest: The authors declare no conflict of interest.

References

1. Mathew, M.M.; Sreelash, K.; Mathew, M.; Arulbalaji, P.; Padmalal, D. Spatiotemporal variability of rainfall and its effect on hydrological regime in a tropical monsoon-dominated domain of Western Ghats, India. *J. Hydrol. Reg. Stud.* **2021**, *36*, 100861. [CrossRef]
2. Ashcroft, L.; Karoly, D.J.; Dowdy, A.J. Historical extreme rainfall events in Southeastern Australia. *Weather Clim. Extrem.* **2019**, *25*, 100210. [CrossRef]
3. Mohan, P.R.; Srinivas, C.; Yesubabu, V.; Baskaran, R.; Venkatraman, B. Simulation of a heavy rainfall event over Chennai in Southeast India using WRF: Sensitivity to microphysics parameterization. *Atmos. Res.* **2018**, *210*, 83–99. [CrossRef]
4. Sun, Q.; Miao, C.; Duan, Q.; Wang, Y. Temperature and precipitation changes over the Loess Plateau between 1961 and 2011, based on high-density gauge observations. *Glob. Planet. Chang.* **2015**, *132*, 1–10. [CrossRef]
5. Onyutha, C. Variability of seasonal and annual rainfall in the River Nile riparian countries and possible linkages to ocean–atmosphere interactions. *Hydrol. Res.* **2016**, *47*, 171–184. [CrossRef]
6. Liu, S.; Qiu, Y.; Fu, R.; Liu, Y.; Suo, C. Identifying the water quality variation characteristics and their main driving factors from 2008 to 2020 in the Yellow River Basin, China. *Environ. Sci. Pollut. Res.* **2023**, *30*, 66753–66766. [CrossRef] [PubMed]
7. Farzana, S.Z.; Paudyal, D.R.; Chadalavada, S.; Alam, M.J. Prediction of Water Quality in Reservoirs: A Comparative Assessment of Machine Learning and Deep Learning Approaches in the Case of Toowoomba, Queensland, Australia. *Geosciences* **2023**, *13*, 293. [CrossRef]
8. Alam, M.J.; Dutta, D. Modelling of nutrient pollution dynamics in river basins: A review with a perspective of a distributed modelling approach. *Geosciences* **2021**, *11*, 369. [CrossRef]
9. Shumway, R.H.; Stoffer, D.S. Time series regression and exploratory data analysis. In *Time Series Analysis and Its Applications: With R Examples*; Springer: Cham, Switzerland, 2017; pp. 45–74. [CrossRef]
10. Almazroui, M.; Şen, Z. Trend analyses methodologies in hydro-meteorological records. *Earth Syst. Environ.* **2020**, *4*, 713–738. [CrossRef]
11. Şen, Z. *Innovative Trend Methodologies in Science and Engineering*; Springer: Cham, Switzerland, 2017.
12. Şen, Z. Innovative trend significance test and applications. *Theor. Appl. Climatol.* **2017**, *127*, 939–947. [CrossRef]
13. Phuong, D.N.D.; Hai, L.M.; Dung, H.M.; Loi, N.K. Temporal trend possibilities of annual rainfall and standardized precipitation index in the Central Highlands, Vietnam. *Earth Syst. Environ.* **2022**, *6*, 69–85. [CrossRef]
14. Imteaz, M.A.; Hossain, I. Climate change impacts on 'seasonality index'and its potential implications on rainwater savings. *Water Resour. Manag.* **2023**, *37*, 2593–2606. [CrossRef]
15. Berihun, M.L.; Tsunekawa, A.; Haregeweyn, N.; Tsubo, M.; Yasuda, H.; Fenta, A.A.; Dile, Y.T.; Bayabil, H.K.; Tilahun, S.A. Examining the past 120 years' climate dynamics of Ethiopia. *Theor. Appl. Climatol.* **2023**, *154*, 535–566. [CrossRef]
16. Fenta, A.A.; Yasuda, H.; Shimizu, K.; Haregeweyn, N.; Kawai, T.; Sultan, D.; Ebabu, K.; Belay, A.S. Spatial distribution and temporal trends of rainfall and erosivity in the Eastern Africa region. *Hydrol. Process.* **2017**, *31*, 4555–4567. [CrossRef]
17. Naddafi, K.; Honari, H.; Ahmadi, M. Water quality trend analysis for the Karoon River in Iran. *Environ. Monit. Assess.* **2007**, *134*, 305–312. [CrossRef]
18. Antonopoulos, V.Z.; Papamichail, D.M.; Mitsiou, K.A. Statistical and trend analysis of water quality and quantity data for the Strymon River in Greece. *Hydrol. Earth Syst. Sci.* **2001**, *5*, 679–692. [CrossRef]
19. Xu, H.; Gao, Q.; Yuan, B. Analysis and identification of pollution sources of comprehensive river water quality: Evidence from two river basins in China. *Ecol. Indic.* **2022**, *135*, 108561. [CrossRef]
20. Xiao, J.; Lv, G.; Chai, N.; Hu, J.; Jin, Z. Hydrochemistry and source apportionment of boron, sulfate, and nitrate in the Fen River, a typical loess covered area in the eastern Chinese Loess Plateau. *Environ. Res.* **2022**, *206*, 112570. [CrossRef]
21. Delpla, I.; Jung, A.-V.; Baures, E.; Clement, M.; Thomas, O. Impacts of climate change on surface water quality in relation to drinking water production. *Environ. Int.* **2009**, *35*, 1225–1233. [CrossRef]
22. Ponting, J.; Kelly, T.J.; Verhoef, A.; Watts, M.J.; Sizmur, T. The impact of increased flooding occurrence on the mobility of potentially toxic elements in floodplain soil—A review. *Sci. Total Environ.* **2021**, *754*, 142040. [CrossRef]
23. Ockenden, M.C.; Hollaway, M.J.; Beven, K.J.; Collins, A.; Evans, R.; Falloon, P.; Forber, K.J.; Hiscock, K.; Kahana, R.; Macleod, C. Major agricultural changes required to mitigate phosphorus losses under climate change. *Nat. Commun.* **2017**, *8*, 161. [CrossRef]
24. Mortazavi-Naeini, M.; Bussi, G.; Elliott, J.A.; Hall, J.W.; Whitehead, P.G. Assessment of risks to public water supply from low flows and harmful water quality in a changing climate. *Water Resour. Res.* **2019**, *55*, 10386–10404. [CrossRef]

25. Watts, G.; Anderson, M. Water Climate Change Impacts Report Card 2016 Edition. Living with Environmental Change. 2016, pp. 9–10. Available online: https://www.ukri.org/wp-content/uploads/2021/12/091221-NERC-LWEC-WaterClimateChangeImpacts-ReportCard2016.pdf (accessed on 8 August 2024).
26. Chen, J.; Gao, Y.; Qian, H.; Jia, H.; Zhang, Q. Insights into water sustainability from a grey water footprint perspective in an irrigated region of the Yellow River Basin. *J. Clean. Prod.* **2021**, *316*, 128329. [CrossRef]
27. Quan, J.; Xu, Y.; Ma, T.; Wilson, J.P.; Zhao, N.; Ni, Y. Improving surface water quality of the Yellow River Basin due to anthropogenic changes. *Sci. Total Environ.* **2022**, *836*, 155607. [CrossRef] [PubMed]
28. Becker, S.; Gemmer, M.; Jiang, T. Spatiotemporal analysis of precipitation trends in the Yangtze River catchment. *Stoch. Environ. Res. Risk Assess.* **2006**, *20*, 435–444. [CrossRef]
29. Gemmer, M.; Fischer, T.; Jiang, T.; Su, B.; Liu, L.L. Trends in precipitation extremes in the Zhujiang River basin, South China. *J. Clim.* **2011**, *24*, 750–761. [CrossRef]
30. Şen, Z. Moving trend analysis methodology for hydro-meteorology time series dynamic assessment. *Water Resour. Manag.* **2024**, 1–15. [CrossRef]
31. Sonali, P.; Kumar, D.N. Review of trend detection methods and their application to detect temperature changes in India. *J. Hydrol.* **2013**, *476*, 212–227. [CrossRef]
32. Sun, W.; Mu, X.; Song, X.; Wu, D.; Cheng, A.; Qiu, B. Changes in extreme temperature and precipitation events in the Loess Plateau (China) during 1960–2013 under global warming. *Atmos. Res.* **2016**, *168*, 33–48. [CrossRef]
33. Tabari, H.; Marofi, S.; Ahmadi, M. Long-term variations of water quality parameters in the Maroon River, Iran. *Environ. Monit. Assess.* **2011**, *177*, 273–287. [CrossRef]
34. Wang, Y.; Xu, Y.; Lei, C.; Li, G.; Han, L.; Song, S.; Yang, L.; Deng, X. Spatio-temporal characteristics of precipitation and dryness/wetness in Yangtze River Delta, eastern China, during 1960–2012. *Atmos. Res.* **2016**, *172*, 196–205. [CrossRef]
35. Westra, S.; Alexander, L.V.; Zwiers, F.W. Global increasing trends in annual maximum daily precipitation. *J. Clim.* **2013**, *26*, 3904–3918. [CrossRef]
36. Zang, C.; Liu, J. Trend analysis for the flows of green and blue water in the Heihe River basin, northwestern China. *J. Hydrol.* **2013**, *502*, 27–36. [CrossRef]
37. Mahmood, R.; Jia, S.; Zhu, W. Analysis of climate variability, trends, and prediction in the most active parts of the Lake Chad basin, Africa. *Sci. Rep.* **2019**, *9*, 6317. [CrossRef] [PubMed]
38. Zhang, Q.; Liu, C.; Xu, C.-y.; Xu, Y.; Jiang, T. Observed trends of annual maximum water level and streamflow during past 130 years in the Yangtze River Basin, China. *J. Hydrol.* **2006**, *324*, 255–265. [CrossRef]
39. Wang, Y.; Xu, Y.; Tabari, H.; Wang, J.; Wang, Q.; Song, S.; Hu, Z. Innovative trend analysis of annual and seasonal rainfall in the Yangtze River Delta, eastern China. *Atmos. Res.* **2020**, *231*, 104673. [CrossRef]
40. Güçlü, Y.S. Multiple Şen-innovative trend analyses and partial Mann-Kendall test. *J. Hydrol.* **2018**, *566*, 685–704. [CrossRef]
41. Dabanlı, İ.; Şen, Z.; Yeleğen, M.Ö.; Şişman, E.; Selek, B.; Güçlü, Y.S. Trend assessment by the innovative-Şen method. *Water Resour. Manag.* **2016**, *30*, 5193–5203. [CrossRef]
42. Hamed, K.H.; Rao, A.R. A modified Mann-Kendall trend test for autocorrelated data. *J. Hydrol.* **1998**, *204*, 182–196. [CrossRef]
43. Miles, K.; Joeland, B.; Bannon, K. *Review of Regional Water Quality and Security 663, Volume 1—Review and Reform Strategy*; Infrastucture Australia: Sydney, NSW, Australia, 2010; pp. 1–68.
44. Wyrwoll, P.R.; Manero, A.; Taylor, K.S.; Rose, E.; Quentin Grafton, R. Measuring the gaps in drinking water quality and policy across regional and remote Australia. *npj Clean Water* **2022**, *5*, 32. [CrossRef]
45. Willems, P.; Olsson, J. *Impacts of Climate Change on Rainfall Extremes and Urban Drainage Systems*; IWA PublishingAlliance House: London, UK, 2012.
46. Queensland Government. Queensland Place Names. Available online: https://www.qld.gov.au/environment/land/title/place-names (accessed on 23 June 2024).
47. Queensland Government. Business Queensland. Available online: https://www.business.qld.gov.au/running-business/support-assistance/mapping-data-imagery/maps/topographic-maps (accessed on 20 June 2024).
48. Amos, M.; Baxter, G.; Finch, N.; Lisle, A.; Murray, P. I just want to count them! Considerations when choosing a deer population monitoring method. *Wildl. Biol.* **2014**, *20*, 362–370. [CrossRef]
49. Bureau of Meteorology. Climate Statistics for Australian Locations. Available online: http://www.bom.gov.au/climate/averages/tables/cw_041103.shtml (accessed on 23 June 2024).
50. Queensland Government. In *Climate Change in the Eastern Downs Regions, Version 1, 2019*; Department of Environment and Science, Queensland Government: Brisbane, QLD, Australia, 2019.
51. Toowoomba Regional Council. Where Our Water Comes from. Available online: https://www.tr.qld.gov.au/environment-water-waste/water-sources-supply-storage-levels/dams-bores/13244-where-our-water-comes-from (accessed on 20 June 2024).
52. Bureau of Meteorology. Climate Glossary. Available online: http://www.bom.gov.au/climate/glossary/seasons.shtml (accessed on 23 June 2024).
53. Oliver, J.E. Monthly precipitation distribution: A comparative index. *Prof. Geogr.* **1980**, *32*, 300–309. [CrossRef]
54. Siqueira, B.; Teixeira Nery, J. Spatial and temporal variability of precipitation concentration in northeastern Brazil. *Investig. Geográficas* **2021**. [CrossRef]
55. Abdi, H. Coefficient of variation. *Encycl. Res. Des.* **2010**, *1*, 169–171.

56. Hare, W. Assessment of knowledge on impacts of climate change–contribution. *Arctic* **2003**, *100*, 25–35.
57. Zaiontz, C. Mann Kendall Test. Available online: https://real-statistics.com/time-series-analysis/time-series-miscellaneous/mann-kendall-test/ (accessed on 23 June 2024).
58. Gedefaw, M.; Yan, D.; Wang, H.; Qin, T.; Girma, A.; Abiyu, A.; Batsuren, D. Innovative trend analysis of annual and seasonal rainfall variability in Amhara regional state, Ethiopia. *Atmosphere* **2018**, *9*, 326. [CrossRef]
59. Gao, F.; Wang, Y.; Chen, X.; Yang, W. Trend analysis of rainfall time series in Shanxi Province, Northern China (1957–2019). *Water* **2020**, *12*, 2335. [CrossRef]
60. Tosunoglu, F. Trend analysis of daily maximum rainfall series in Çoruh Basin, Turkey. *J. Inst. Sci. Technol.* **2017**, *7*, 195–205. [CrossRef]
61. Sen, P.K. Estimates of the regression coefficient based on Kendall's tau. *J. Am. Stat. Assoc.* **1968**, *63*, 1379–1389. [CrossRef]
62. Şen, Z. Innovative trend analysis methodology. *J. Hydrol. Eng.* **2012**, *17*, 1042–1046. [CrossRef]
63. Pour, S.H.; Abd Wahab, A.K.; Shahid, S.; Ismail, Z.B. Changes in reference evapotranspiration and its driving factors in peninsular Malaysia. *Atmos. Res.* **2020**, *246*, 105096. [CrossRef]
64. Şen, Z.; Şişman, E.; Dabanli, I. Innovative polygon trend analysis (IPTA) and applications. *J. Hydrol.* **2019**, *575*, 202–210. [CrossRef]
65. Ebrahimi, A.; Rahimi, D.; Joghataei, M.; Movahedi, S. Correlation wavelet analysis for linkage between winter precipitation and three oceanic sources in Iran. *Environ. Process.* **2021**, *8*, 1027–1045. [CrossRef]
66. Vacha, L.; Barunik, J. Co-movement of energy commodities revisited: Evidence from wavelet coherence analysis. *Energy Econ.* **2012**, *34*, 241–247. [CrossRef]
67. Grinsted, A.; Moore, J.C.; Jevrejeva, S. Application of the cross wavelet transform and wavelet coherence to geophysical time series. *Nonlinear Process. Geophys.* **2004**, *11*, 561–566. [CrossRef]
68. Torrence, C.; Compo, G.P. A practical guide to wavelet analysis. *Bull. Am. Meteorol. Soc.* **1998**, *79*, 61–78. [CrossRef]
69. Torrence, C.; Webster, P.J. Interdecadal changes in the ENSO–monsoon system. *J. Clim.* **1999**, *12*, 2679–2690. [CrossRef]
70. Das, J.; Mandal, T.; Rahman, A.S.; Saha, P. Spatio-temporal characterization of rainfall in Bangladesh: An innovative trend and discrete wavelet transformation approaches. *Theor. Appl. Climatol.* **2021**, *143*, 1557–1579. [CrossRef]
71. Queensland Government. *Queensland's Extended Wet and Dry Periods*; Ecosciences Precinct, Queensland Government: Brisbane, QLD, Australia, 2019.
72. Yang, Q.; Chen, J.; Liu, Y.; Li, Y.; Zhang, H.; Zhang, J.; Sun, X.; Lu, M.; Ma, R.; Wu, Y. Analysis of changes in water quality and treatment effectiveness of seven major river basins in China from 2001 to 2020. *Front. Environ. Sci.* **2024**, *12*, 1340994. [CrossRef]